Supplementary Information (SI)

Peripheral Halogenation Engineering Controls Molecular Stacking to Enable Highly Efficient Organic Solar Cells

Yalu Zou,[†][a] Hongbin Chen,[†][a] Xingqi Bi,[a] Xiaoyun Xu,[b] Hebin Wang,[c] Menglu Lin,[c] Zaifei Ma,[b] Mingtao Zhang,[a] Chenxi Li,[a] Xiangjian Wan,[a] Guankui Long,[c, d] Zhaoyang Yao,*[a] Yongsheng Chen*[a]

[a] The State Key Laboratory and Institute of Elemento-Organic Chemistry, Centre of Nanoscale Science and Technology, Key Laboratory of Functional Polymer Materials, Renewable Energy Conversion and Storage Center (RECAST), College of Chemistry, Nankai University, Tianjin 300071, China.

[b] The State Key Laboratory for Modification of Chemical Fibers and Polymer Materials, Center for Advanced Low-dimension Materials, College of Materials Science and Engineering, Donghua University, Shanghai, 201620, China.

[c] The National Institute for Advanced Materials, Renewable Energy Conversion and Storage Center (RECAST), College of Materials Science and Engineering, Nankai University, Tianjin, 300350, China.

[d] The State Key Laboratory of Luminescent Materials and Devices, South China University of Technology, Guangzhou, 510640, China

[†] These authors contributed equally: Yalu Zou, Hongbin Chen.

E-mail: yschen99@nankai.edu.cn; zyao@nankai.edu.cn

CONTENTS

1. Experimental Section 3

1.1 Materials 3

1.2 Single-Crystal Growth 3

1.3 Device Fabrication and Measurement 4

1.4 UV-Visible (UV-Vis) Absorption 5

1.5 Thermogravimetric Analysis (TGA) and Cyclic Voltammetry (CV) 5

1.6 Atomic Force Microscopy (AFM) and Transmission Electron Microscopy (TEM) 5

1.7 Grazing Incidence Wide Angle X-Ray Scattering (GIWAXS) and the Contact Angles 5

1.8 Photoluminescence (PL) 6

1.9 Electroluminescence (EL) and Electroluminescence EQE (EQE_{EL}) 6

1.10 Highly Sensitive EQE (sEQE) 6

1.11 Space-Charge-Limited Current (SCLC) Measurement 7

1.12 Measurements of Transient Photovoltage (TPV)/Transient Photocurrent (TPC) 7

2. Synthetic Section and Supporting Schemes 7

3. Supporting Figures and Tables 12

4. Supporting Notes 46

5. ^{1}H and ^{13}C NMR Spectra of the Key Intermediates and Final Products 50

References 58

1. Experimental Section

1.1 Materials

The polymeric donor **PM6**, starting material **1**, **INCN-2F** and **INCN-2Cl** were purchased from Solarmer Material (Beijing) Inc, eFlexPV Limited and Senior material, respectively. The control molecule **Y6** was synthesized according to the reported method by Zou et al.[1] The polymeric donor **D18** was synthesized according to the reported method by Ding et al.[2] **F-2F** was synthesized according to our previously reported method.[3] The pre-patterned ITO glass and the mask used for depositing metal electrodes were purchased from Advanced Election Technology Co., Ltd. All solutions were stirred at room temperature for 12 h and filtered with a 0.22 μm PTFE filter prior to use. All the other reagents and chemicals were purchased from commercial suppliers and were used directly without further purification. The detailed synthesized procedures of **CH-4Cl**, **CH-6F** and **CH-6Cl** and their characterizations were displayed below.

1.2 Single-Crystal Growth

Single crystals of **CH-6F**, **CH-4Cl** and **CH-6Cl** were grown by the liquid diffusion method at room temperature. In detail, 1.5 mL of n-hexane or methanol was transferred to 0.15 mL of a concentrated chloroform solution of **CH-6F**, **CH-4Cl** and **CH-6Cl** slowly, and the beautiful cuboid-shape dark purple crystals were formed on the inner glassy tube after about 10 days. The X-ray diffraction signals of single crystal were collected on Rigaku XtalAB PRO MM007 DW. The crystal was kept at 173.0 K during data collection. The detailed crystal parameters of the three crystals were summarized in **Table S1**.

1.3 Device Fabrication and Measurement

The conventional devices based on **PM6**:**CH**-series NFAs (**CH-6F**, **CH-4Cl** and **CH-6Cl**) were fabricated with an architecture of ITO/PEDOT:PSS/**PM6**:**CH**-series/PNDIT-F3N/Ag. In detail, the ITO glass was pre-cleaned in turn in an ultrasonic bath of detergent, deionized water, acetone, and isopropanol. Then the surface of ITO was treated with UV light in an ultraviolet-ozone chamber (Jelight Company) for 15 min. A thin layer of poly(3,4-ethylene dioxythiophene):poly(styrene sulfonate) (PEDOT:PSS, Baytron PVP Al 4083) was prepared by spin-coating the PEDOT:PSS solution at 4300 rpm for 20 s on the ITO substrate. Note that the PEDOT:PSS solution was pre-filtered through a 0.45 mm poly(tetrafluoroethylene) (PTFE) filter. Subsequently, the PEDOT:PSS films were baked at 150 ℃ for 20 min in air and transferred to a glove box filled with argon. Then the **PM6**:**CH**-series mixtures (D:A ratio=1:1) were fully dissolved in chloroform (CF) with 0.3% 1-chloronaphthalene (CN) as an additive at a total concentration of 14 mg/mL and the resulting solutions were spin-casted at 2100 rpm for 30 s onto the PEDOT:PSS layer. After that, about 20 nm thickness of PNDIT-F3N (dissolved in methanol with 0.3% *v*/*v* glacial acetic acid at the concentration of 1.5 mg/mL) layer was spin-coated on the top of the active layer. Finally, a layer of Ag with a thickness of 150 nm was deposited under 2×10^{-6} Pa. The active area of the device was 4 mm^2.

The current density-voltage (*J*-*V*) curves of photovoltaic devices were recorded by a Keithley 2400 source-measure unit. The photocurrent was measured under the simulated illumination of 100 mW cm^{-2} with AM1.5 G using an Enli SS-F5-3A solar simulator, which was calibrated by a standard Si solar cell (made by Enli Technology Co., Ltd., Taiwan, and calibrated report can be traced to NREL). The thickness of the active layers was measured by a Veeco Dektak 150 profilometer. The EQE spectra were measured by using a QE-R Solar Cell Spectral Response Measurement System (Enli Technology Co., Ltd., Taiwan).

1.4 UV-Visible (UV-Vis) Absorption

UV-vis spectra were obtained by a Cary 5000 UV-vis spectrophotometer. The diluted solutions of **CH-6F**, **CH-4Cl** and **CH-6Cl** were kept at a low concentration of 10^{-5} M.

1.5 Thermogravimetric Analysis (TGA)and Cyclic Voltammetry (CV)

The TGA was carried out on a NETZSCH STA 409PC instrument under purified nitrogen gas flow. The heating rate is 10 °C min^{-1}. The CV experiments were performed with an LK98B II Microcomputer-based Electrochemical Analyzer. All measurements were conducted at room temperature with a three-electrode configuration. Among them, a glassy carbon electrode was employed as the working electrode, a saturated calomel electrode (SCE) was used as the reference electrode, and a Pt wire was used as the counter electrode. Tetrabutyl ammonium phosphorus hexafluoride (*n*-Bu_4NPF_6, 0.1 M) in acetonitrile was employed as the supporting electrolyte, and the scan rate was kept at 100 Mv s^{-1}. Electrochemically reversible ferrocene was employed as an internal reference. The HOMO and LUMO energy levels were calculated from the onset oxidation and the onset reduction potentials, respectively, by following the equation E_{HOMO}= –(4.80+E_{ox}^{onset}) eV, E_{LUMO}= –(4.80+E_{re}^{onset}) eV.

1.6 Atomic Force Microscopy (AFM) and Transmission Electron Microscopy (TEM)

The AFM images were performed using tapping mode on a Bruker Dimension Icon atomic force microscope. The TEM was performed on a Talos F200X G2.

1.7 Grazing Incidence Wide Angle X-Ray Scattering (GIWAXS) and the Contact Angles

The GIWAXS samples were deposited on Si substrates by use of the same preparation conditions with devices and were carried out with XEUSS SAXS/WAXS equipment. The contact angles were measured using a JC2000D1 contact angle instrument.

1.8 Photoluminescence (PL)

The PL measurements were conducted by using FLS1000 equipment. The emission spectra and PLQY of **CH-6F**, **CH-4Cl** and **CH-6Cl** were obtained using the same setup used for recording electroluminescence spectra excited by an 825 nm wavelength provided by a Xenon lamp (Detector for NIR 5509 PMT, 600~1700nm).

1.9 Electroluminescence (EL) and Electroluminescence External Quantum Efficiency (EQE_{EL})

The EL measurements were carried out by using a source meter (Keithley 2400) to inject electric current, and the emitted photons were measured using a fluorescence spectrometer (KYMERA-328I-B2, Andor technology LTD) with a Si EMCCD camera (DU491A-1.7, Andor). The injection current to the OSCs was kept at 1 mA by the direct current meter (PWS2326 Tectronix). For the EQE_{EL} measurements, a digital source meter (Keithley 2400) was employed to inject electric current into the solar cells, and the emitted photons were collected by a Si diode (Hamamatsu s1337-1010BQ) and indicated by a picometer (Keithley 6482). All the EQE-EL measurements were conducted at 298 K.[4]

1.10 Highly Sensitive EQE (sEQE)

sEQE measurements were conducted by using a measurement system containing a halogen lamp light source (LSH-75, Newport), and a monochromator (CS260-RG-3-MC-A, Newport), a current amplifier, a chopper, and a phase-locked amplifier (SR830, Newport). The overtone signals from the monochromator were blocked by a group of long pass filters (1100 nm, 900 nm, 600 nm).

1.11 Space-Charge-Limited Current (SCLC) Measurement

The SCLC method was used to measure the hole and electron mobilities, by using a diode configuration of ITO/PEDOT:PSS/active layer/MoO_3/Al for hole and ITO/ZnO/active layer/PNDIT-F3N/Al for electron. The dark current density curves were recorded with a bias voltage in the range of 0~8 V. The mobilities were estimated by taking current-voltage curves and fitting the results based on the equation listed below:

$$J=\frac{9\varepsilon_0\varepsilon_\gamma\mu V^2}{8L^3}$$

where J is the current density, ε_0 is the vacuum permittivity, ε_r is the relative dielectric constant, μ is the mobility, and L is the film thickness. V (V_{app}–V_{bi}) is the internal voltage in the device, where V_{app} is the applied voltage to the device and V_{bi} is the built-in voltage due to the relative work function difference between the two electrodes.

1.12 Measurements of Transient Photovoltage (TPV)/Transient Photocurrent (TPC)

A white light bias was generated from an array of diodes (Molex 180081-4320) with light intensity about 0.5 sun. The light intensity of the diode pumped laser passing through an attenuator is about 1132.5 μW/cm^2. A diode pumped laser (Lapa-80) was used as the perturbation source, with a pulse duration of 10 ns and a repetition frequency of 20 Hz. The perturbation light intensity was attenuated to keep the amplitude of transient V_{OC} (ΔV_{OC}) below 10 mV so that $\Delta V_{OC} << V_{OC}$. Voltage and current dynamics were recorded on a digital oscilloscope (Tektronix MDO4104C), and voltages at open circuit and currents under short circuit conditions were measured over a 1 MΩ and a 50 Ω resistor, respectively.

2. Synthetic Section and Supporting Schemes

Synthesis of CHs.

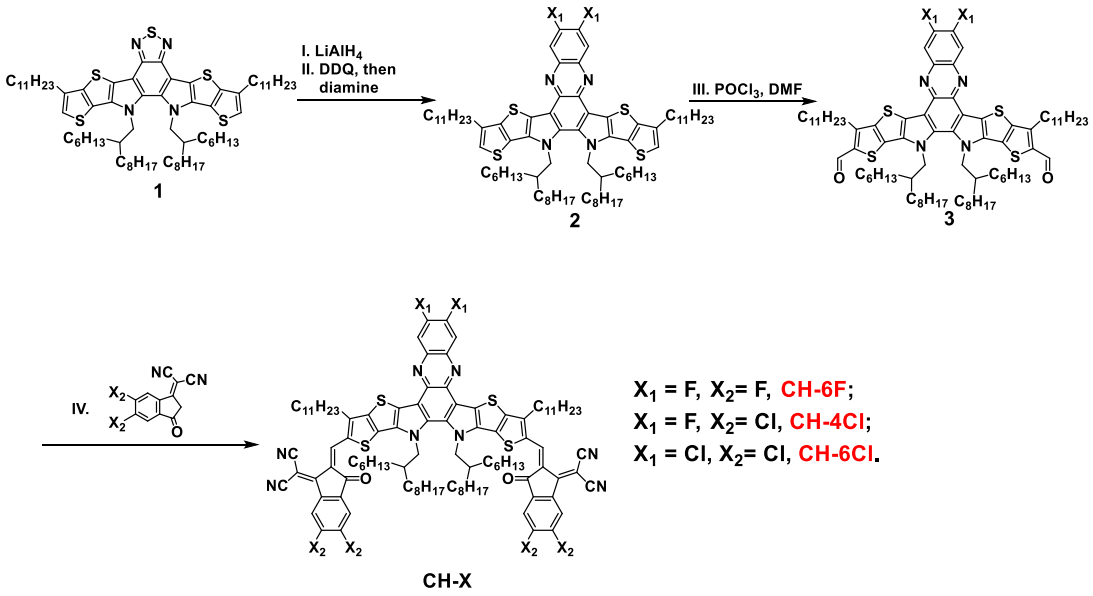

Scheme S1. The overall synthetic route to CH-series. Reagents and conditions: (I) $LiAlH_4$, THF, reflux; (II) DDQ, $CHCl_3$, then 4,5-difluorobenzene-1,2-diamine or 4,5-dichlorobenzene-1,2-diamine, 0 °C to room temperature; (III) $POCl_3$, DMF, $ClCH_2CH_2Cl$, reflux; (IV) 2-(6,7-difluoro-3-oxo-2,3-dihydro-1H-cyclopenta[b] naphthalen-1-ylidene) malononitrile or 2-(5,6-dichloro-3-oxo-2,3-dihydro-1H-inden-1-ylidene) malononitrile, pyridine, $CHCl_3$, reflux.

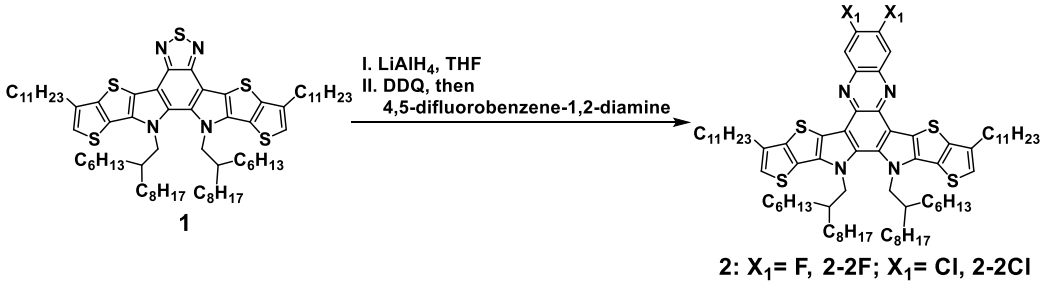

Scheme S2. Synthesis of compound 2. Under the protection of argon, $LiAlH_4$ (119 mg, 3.14 mmol, 5.0 eq.) was added to a solution of compound **1** (750 mg, 0.63 mmol, 1.0 eq.) in tetrahydrofuran (THF, 50 mL). The resulting mixture was stirred and heated to reflux for 12 h. After being cooled to 0 ℃, water (30 mL) is slowly dropped into the reaction and extracted with dichloromethane. The organic layer was dried over anhydrous Na_2SO_4 for 1 h. After removal of solvent, the crude product was dissolved in chloroform (45 mL), then 3-dichloro-5,

6-dicyano-1, 4-benzoquinone (DDQ, 285 mg, 1.26 mmol, 2.0 eq.) and 5-difluorobenzene-1,2-diamine (452 mg, 3.14 mmol, 5.0 eq.) were added to the solution in turn. The reaction was stirred at room temperature for 6 h, and the solvent was removed under vacuum. Finally, the residue was purified by column chromatography to give compound **2-2F** as a red solid. (625 mg, 78%). Compound **2-2Cl** is obtained by a similar method with a yield of 75% as a red solid.

Data for compound **2-2F**: **^{1}H NMR** (400 MHz, $CDCl_3$) δ 8.17 (t, *J*=9.3 Hz, 1H), 7.03 (s, 1H), 4.67 (d, *J*=6.6 Hz, 2H), 2.87 (s, 2H), 2.16 (s, 1H), 1.90 (s, 2H), 1.54-1.24 (m, 17H), 1.15-0.87 (m, 24H), 0.72-0.83 (m, 5H), 0.67 (t, *J*=6.2 Hz, 3H). **^{13}C NMR** (101 MHz, $CDCl_3$) δ 153.0, 150.4, 143.1, 138.4, 138.2, 136.9, 131.6, 123.5, 123.3, 119.2, 116.7, 114.3, 55.1, 38.7, 32.0, 31.8, 31.6, 30.5, 30.4, 29.8, 29.7, 29.6, 29.5, 29.4, 29.4, 29.4, 29.2, 29.0, 25.5, 22.7, 22.6, 22.5, 14.2, 14.1, 14.0. MS (*m*/*z*, MALDI): Calc. for $C_{78}H_{116}F_2N_4S_4$ $[M+H]^+$ 1275.81, found: 1275.78.

Data for compound **2-2Cl**: **^{1}H NMR** (400 MHz, $CDCl_3$) δ 8.51 (s, 1H), 7.03 (s, 1H), 4.70 (d, *J*=7.1 Hz, 2H), 2.86 (t, *J*=7.6 Hz, 2H), 2.21 (s, 1H), 1.97-1.78 (m, 2H), 1.49-0.88 (m, 42H), 0.80 (t, *J*=7.2 Hz, 4H), 0.68 (t, *J*=6.8 Hz, 3H). **^{13}C NMR** (101 MHz, $CDCl_3$) δ 143.2, 139.8, 138.9, 137.0, 136.9, 132.1, 131.8, 129.6, 123.5, 123.4, 119.0, 116.7, 55.0, 38.7, 32.0, 31.8, 31.7, 30.5, 30.5, 29.8, 29.6, 29.5, 29.2, 28.9, 25.6, 22.8, 22.6, 22.5, 14.2, 14.2, 14.0. Calc. for C78H116Cl2N4S4 [M]+ 1306.75, found: 1306.81.

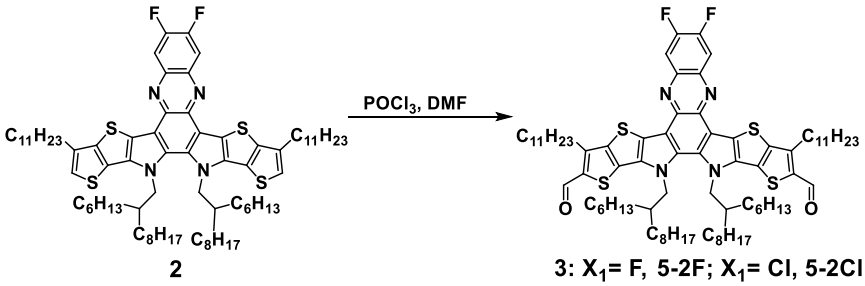

Scheme S3. Synthesis of compound 3. Under the protection of argon, phosphorus oxychloride (0.3 mL) was added to a solution of compound **2** (550 mg) and N, N-Dimethylformamide (DMF, 0.3 mL) in 1, 2-dichloroethane ($ClCH_2CH_2Cl$, 50 mL). The

resulting mixture was stirred and heated to reflux for 12 h, then cooled to 0 ℃. The resulting mixture was slowly added to a saturated solution of sodium acetate (40 mL), then stirred at room temperature for 2 h. The resulting mixture was extracted with dichloromethane and the organic layer was dried over anhydrous Na_2SO_4 for 1 h. After removal of solvent, the crude product was then purified by column chromatography on silica gel with hexanes/dichloromethane (*v*/*v*=1:2) as eluent to afford compound **3-2F** as a red solid (495 mg, 86%). Compound **2-2Cl** is obtained by a similar method with a yield of 82% as a red solid.

Data for compound **3-2F**: **^{1}H NMR** (400 MHz, $CDCl_3$) δ 10.16 (s, 1H), 8.13 (t, *J*=9.5 Hz, 1H), 4.70 (d, *J*=7.7 Hz, 2H), 3.24 (t, *J*=7.6 Hz, 2H), 2.14 (s, 1H), 2.05-1.85 (m, 2H), 1.58-1.47 (m, 2H), 1.35-1.41 (m, 2H), 1.25-1.36 (m, 13H), 1.14-0.81 (m, 26H), 0.76 (t, *J*=7.2 Hz, 3H), 0.66 (t, *J*=6.9 Hz, 3H). **^{13}C NMR** (101 MHz, $CDCl_3$) δ 181.7, 153.3, 151.0, 146.9, 144.2, 138.9, 138.1, 136.9, 136.8, 132.8, 129.5, 128.0, 117.6, 114.3, 55.4, 39.0, 31.9, 31.8, 31.6, 30.5, 30.5, 30.4, 29.7, 29.6, 29.6, 29.4, 29.4, 29.3, 29.1, 28.2, 25.5, 22.7, 22.6, 22.5, 14.1, 14.1, 13.9. MS (*m*/*z*, MALDI): Calc. for $C_{80}H_{116}F_2N_4O_2S_4$ $[M+H]^+$ 1331.80, found: 1331.64.

Data for compound **3-2Cl**:**^{1}H NMR** (400 MHz, $CDCl_3$) δ 10.13 (s, 1H), 8.31 (s, 1H), 4.70 (d, *J*=7.6 Hz, 2H), 3.15 (t, *J*=7.4 Hz, 2H), 2.18 (s, 1H), 1.98-1.80 (m, 2H), 1.50-1.40 (m, 2H), 1.37-0.84 (m, 41H), 0.72 (t, *J*=7.2 Hz, 3H), 0.65 (t, *J*=6.8 Hz, 3H). **^{13}C NMR** (101 MHz, $CDCl_3$) δ 181.7, 146.8, 144.3, 139.9, 138.5, 136.9, 136.7, 133.0, 132.7, 129.4, 129.3, 128.0, 117.5, 55.5, 39.1, 31.9, 31.8, 31.6, 30.6, 30.5, 29.8, 29.7, 29.7, 29.6, 29.5, 29.5, 29.4, 29.2, 28.2, 25.7, 25.7, 22.7, 22.6, 22.5. MS (*m*/*z*, MALDI): Calc. for $C_{80}H_{116}Cl_2N_4O_2S_4$ $[M]^+$ 1362.74, found: 1362.76.

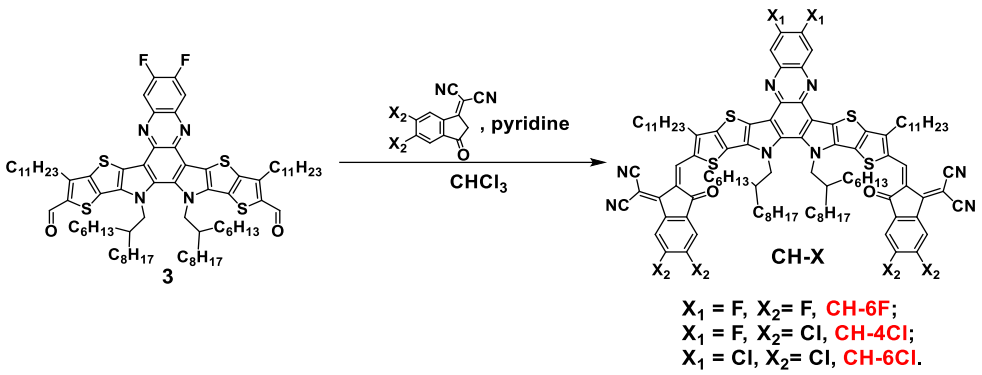

Scheme S4. Synthesis of compound CH-series. Under the protection of argon, dry pyridine (0.5 mL) was added to a solution of compound **3-2F** (450 mg, 0.338 mmol, 1.0 eq.) and 2-(5,6-difluoro-3-oxo-2,3-dihydro-1H-inden-1-ylidene) malononitrile (232 mg, 1.01 mmol 3.0 eq.) in chloroform ($CHCl_3$, 45 mL). The resulting mixture was stirred and heated to reflux for 12 h. After being cooled to room temperature, the solvent was removed under a vacuum. The crude product was then purified by column chromatography on silica gel with hexanes/dichloromethane (*v*/*v*=1:3) as eluent to afford **CH-6F** as a black and blue solid (534 mg, 90%). Compound **CH-4Cl** is obtained by a similar method with a yield of 86% as a black and blue solid. Compound **CH-6Cl** is also obtained by a similar method with a yield of 82% as a black and blue solid.

Data for **CH-6F**: **^{1}H NMR** (400 MHz, $CDCl_3$) δ 9.18 (s, 1H), 8.58 (dd, *J*=9.8, 6.2 Hz, 1H), 8.17 (t, *J*=9.2 Hz, 1H), 7.71 (t, *J*=7.5 Hz, 1H), 4.81 (d, *J*=7.6 Hz, 2H), 3.29 (t, *J*=7.6 Hz, 2H), 2.20 (s, 1H), 1.95-1.85 (m, 2H), 1.63-1.47 (m, 4H), 1.43-0.97 (m, 35H), 0.86 (t, *J*=6.8 Hz, 4H), 0.75 (t, *J*=7.2 Hz, 3H), 0.66 (t, *J*=6.8 Hz, 3H). **^{13}C NMR** (101 MHz, $CDCl_3$) δ 186.1, 158.4, 155.7, 155.6, 154.0, 153.2, 153.0, 151.2, 151.0, 146.2, 138.9, 137.9, 137.8, 136.6, 135.9, 135.0, 134.5, 133.7, 133.1, 131.5, 119.6, 118.8, 115.0, 114.7, 114.4, 112.2, 68.0, 56.1, 39.2, 31.9, 31.9, 31.7, 31.4, 30.8, 30.7, 29.9, 29.7, 29.7, 29.6, 29.6, 29.4, 29.4, 29.2, 25.9, 25.8, 22.7, 22.6, 22.5, 14.1, 14.1, 14.0. HRMS (*m*/*z*, MALDI): Calc. for $C_{104}H_{121}F_6N_8O_2S_4$ $[M+H]^+$ 1755.8394, found: 1755.9394 (HRMS: high resolution mass spectrum).

Data for **CH-4Cl**: **^{1}H NMR** (400 MHz, $CDCl_3$) δ 9.21 (s, 1H), 8.80 (s, 1H), 8.17 (t, *J*=9.3 Hz, 1H), 7.97 (s, 1H), 4.81 (d, *J*=7.7 Hz, 2H), 3.29 (t, *J*=7.6 Hz, 2H), 2.20 (s, 1H), 1.95-1.85 (m, 2H), 1.62-1.53 (m, 2H), 1.41-0.96 (m, 37H), 0.86 (t, *J*=6.7 Hz, 4H), 0.75 (t, *J*=7.2 Hz, 3H), 0.67 (t, *J*=6.7 Hz, 3H). **^{13}C NMR** (101 MHz, $CDCl_3$) δ 186.2, 158.2, 154.1, 153.8, 153.6, 151.3, 151.1, 146.5, 139.4, 139.1, 138.8, 138.6, 137.9, 137.8, 136.3, 136.0, 135.3, 133.8, 133.6, 131.6, 126.7, 126.7, 124.9, 124.9, 119.4, 118.9, 115.1, 114.4, 114.2, 68.2, 55.9, 39.6, 31.9, 31.9, 31.7, 31.4, 30.8, 30.0, 30.0, 29.8, 29.7, 29.7, 29.6, 29.5, 29.4, 29.3, 25.9, 22.7, 22.6, 22.6, 14.1. HRMS (*m*/*z*, MALDI): Calc. for $C_{104}H_{121}Cl_4F_2N_8O_2S_4$ $[M+H]^+$ 1819.7212, found: 1819.7203.

Data for **CH-6Cl**: **^{1}H NMR** (400 MHz, $CDCl_3$) δ 9.21 (s, 1H), 8.88 (s, 1H), 8.53 (s, 1H), 8.00 (s, 1H), 4.85 (d, *J*=7.6 Hz, 2H), 3.29 (t, *J*=7.8 Hz, 2H), 2.25 (s, 1H), 1.93 (s, 2H), 1.46-0.92 (m, 43H), 0.77 (t, *J*=7.2 Hz, 3H), 0.69 (t, *J*=6.8 Hz, 1H). **^{13}C NMR** (101 MHz, $CDCl_3$) δ 186.2, 158.4, 154.1, 146.6, 140.0, 140.0, 139.6, 139.3, 138.7, 138.5, 137.7, 136.2, 136.0, 135.6, 133.6, 131.8, 129.3, 126.8, 125.0, 119.7, 118.8, 115.1, 114.5, 68.4, 56.0, 39.6, 31.9, 31.9, 31.7, 31.4, 30.9, 30.0, 29.7, 29.7, 29.6, 29.5, 29.4, 29.3, 26.0, 22.7, 22.6, 22.5, 14.1, 14.1. HRMS (*m*/*z*, MALDI): Calc. for $C_{104}H_{121}Cl_6N_8O_2S_4$ $[M+H]^+$ 1851.6621, found: 1851.6624.

3. Supporting Figures and Tables

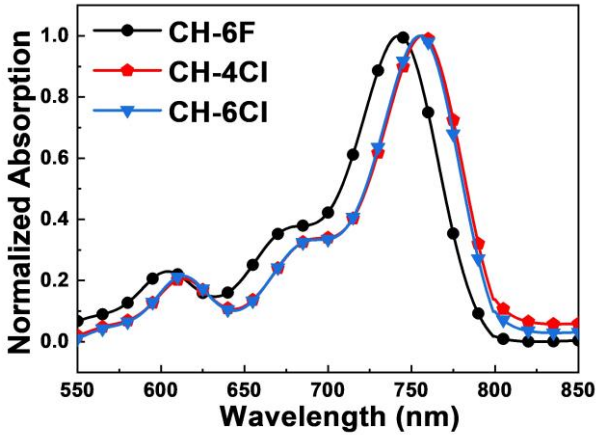

Figure S1. Normalized absorption spectra of CH-6F, CH-4Cl and CH-6Cl in dilute chloroform solutions.

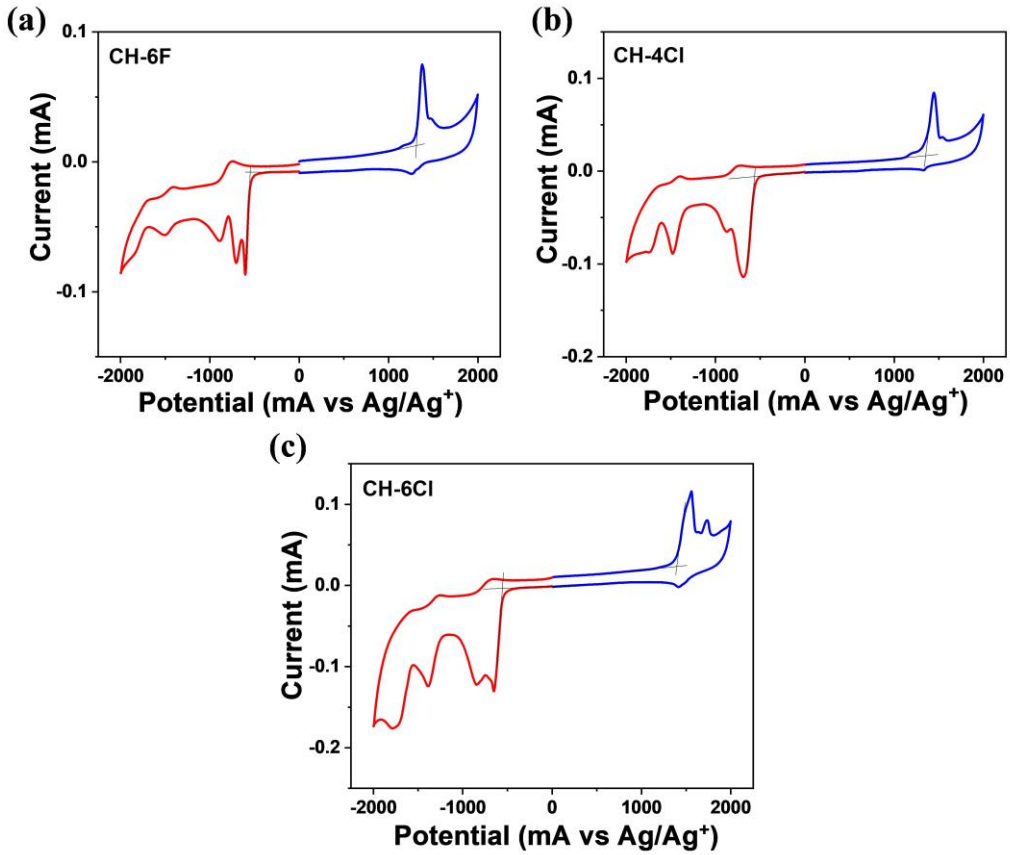

Figure S2. Cyclic voltammograms of (a) CH-6F, (b) CH-4Cl and (c) CH-6Cl films. Red line: oxidation cycle, blue line: reduction cycle.

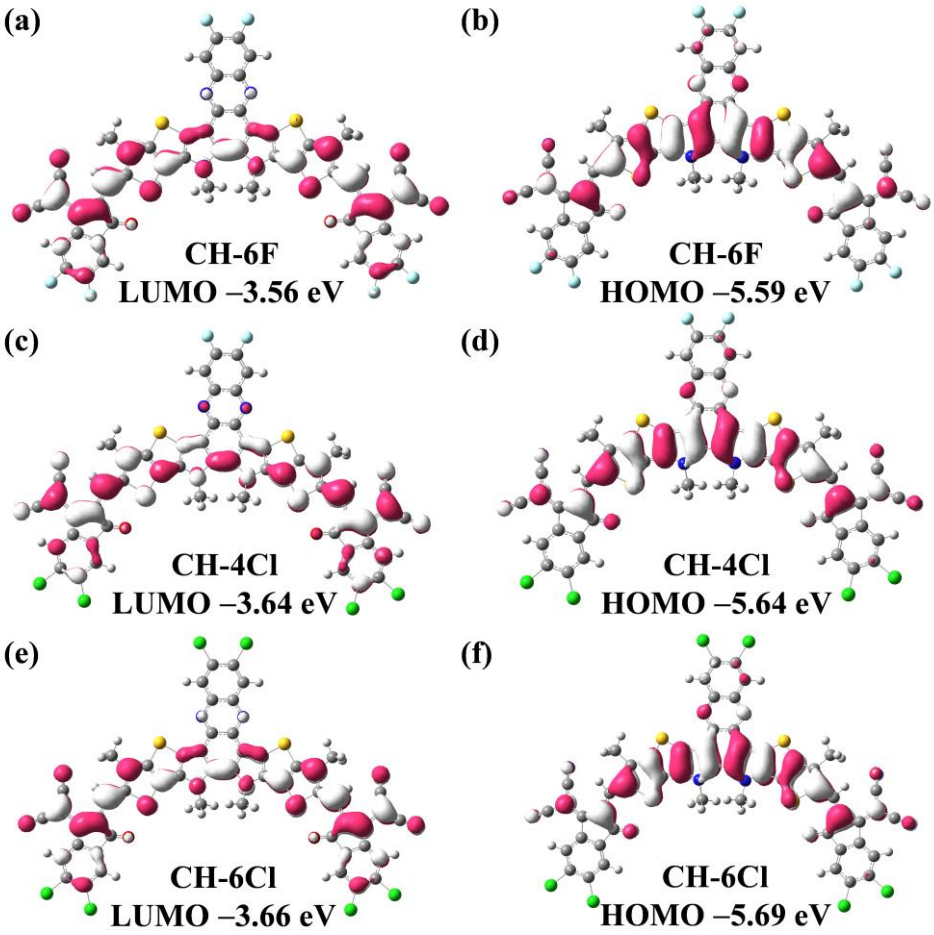

Figure S3. Theoretical density distribution for the frontier molecular orbits of (a, b) CH-6F, (c, d) CH-4Cl and (e, f) CH-6Cl. Note that the relative alignment of energy levels derived from CVs (**Table 1**) is in accordance with the results from theoretical calculations.

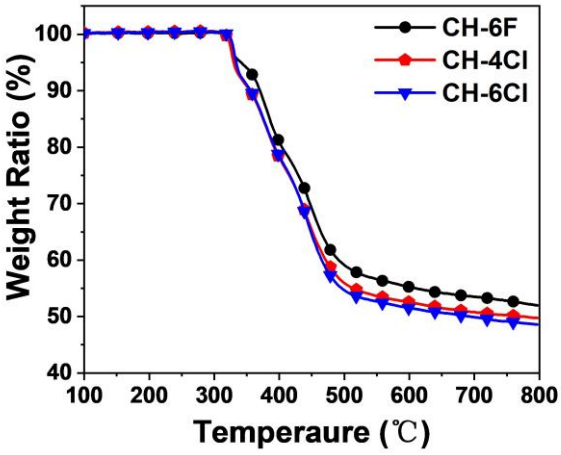

Figure S4. Thermogravimetric analysis (TGA) curves of CH-6F, CH-4Cl and CH-6Cl acceptors, respectively. The heating rate is 10 ºC/min under a nitrogen atmosphere.

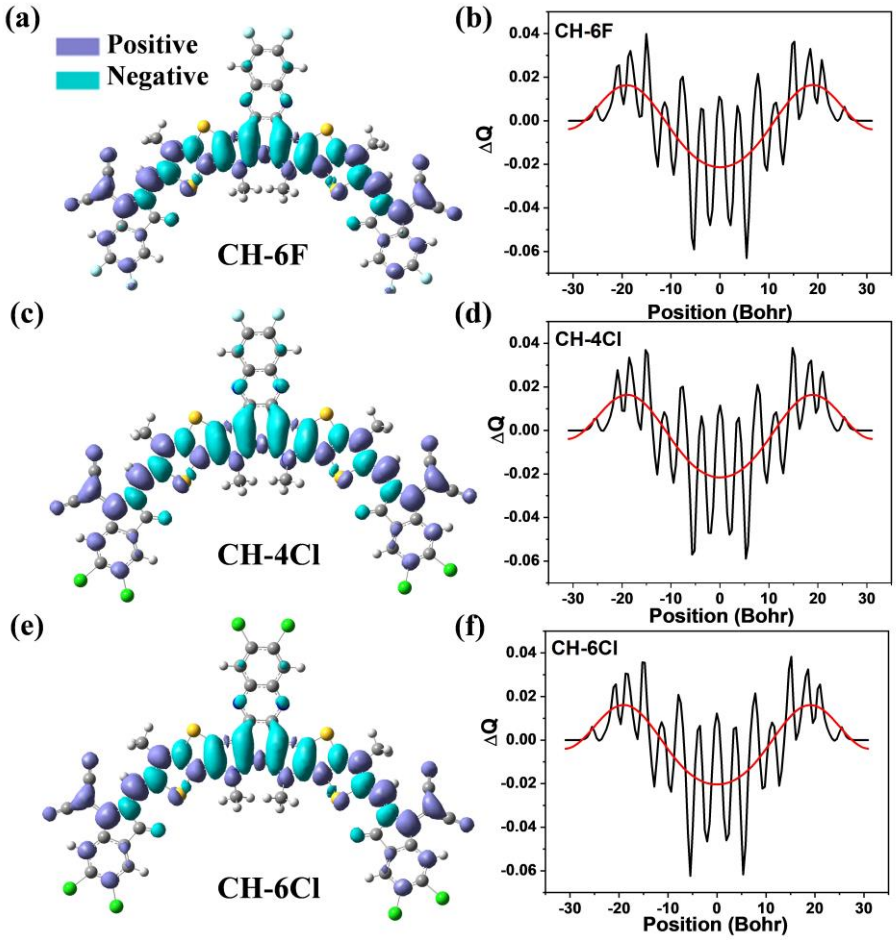

Figure S5. Theoretical density distribution ΔQ ($\Delta Q=\Psi^2_{LUMO}-\Psi^2_{HOMO}$) along the longest axis (backbone) of (a, b) CH-6F, (c, d) CH-4Cl and (e, f) CH-6Cl. Charge density difference ΔQ ($\Delta Q=\Psi^2_{LUMO}-\Psi^2_{HOMO}$) along the longest axis (backbone) of the defined molecules.[5] Black curves are the integral lines of the charge density difference (ΔQ) along the longest axis (backbone) of the defined molecules. Red curves are the simulated results with low frequencies wave functions by fast flourier transform filters.

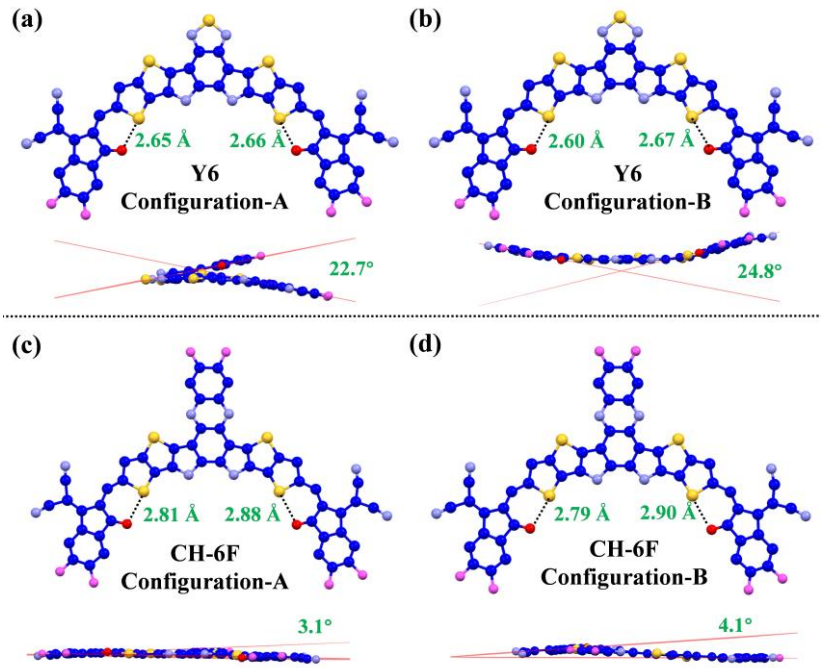

Figure S6. The monomolecular single crystallographic structures of (a-b) Y6 and (c-d) CH-6F with two configurations in top-view and side-view. The alkyl chains and hydrogen atoms are omitted for clarity, $d_{S\text{-}O}$=the length of the S···O interaction.

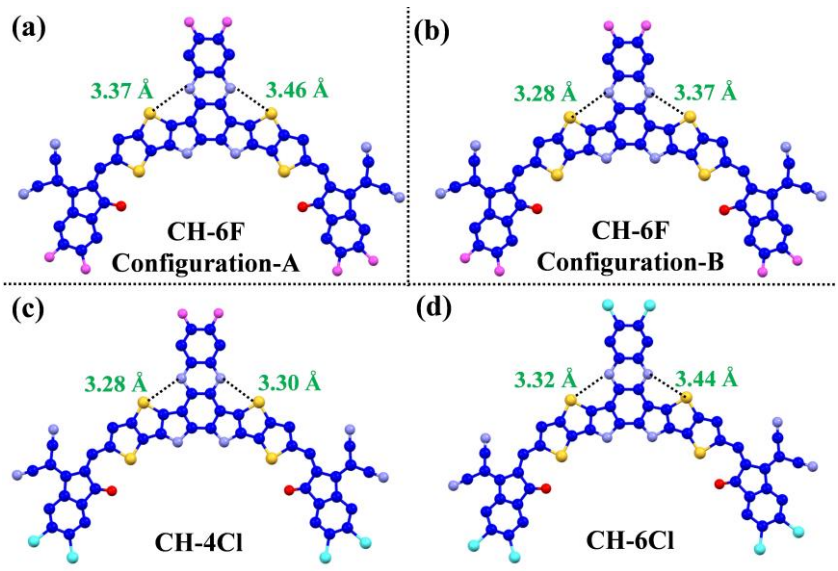

Figure S7. The monomolecular single crystallographic structures of (a-b) CH-6F, (c) CH-4Cl and (d) CH-6Cl in top-view. The alkyl chains and hydrogen atoms are omitted for clarity.

d_{S-N}=the length of the S···N interaction; Configuration-A and Configuration-B represent two different configurations of **CH-6F**, **CH-4Cl** and **CH-6Cl** have only one configuration.

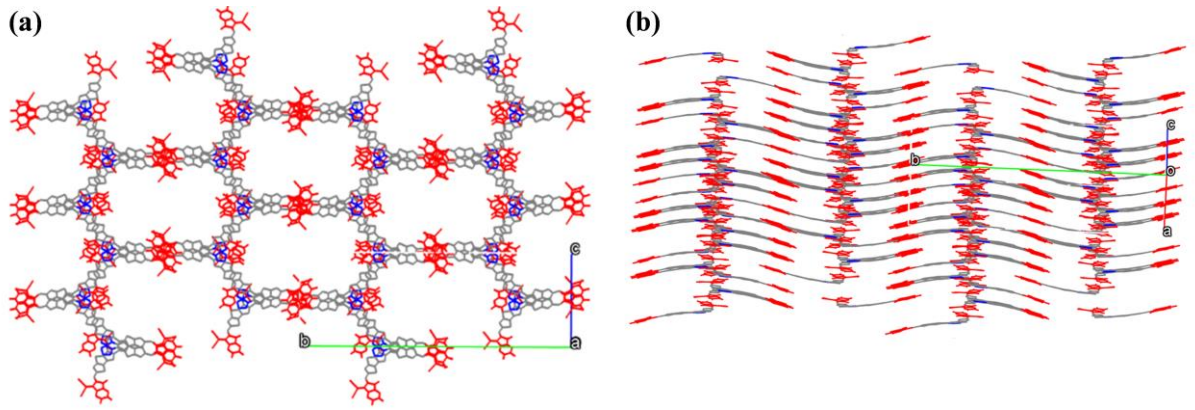

Figure S8. Single-crystal packing diagrams from the (a) top view and (b) side view of Y6. The alkyl chains and hydrogen atoms are omitted for clarity.

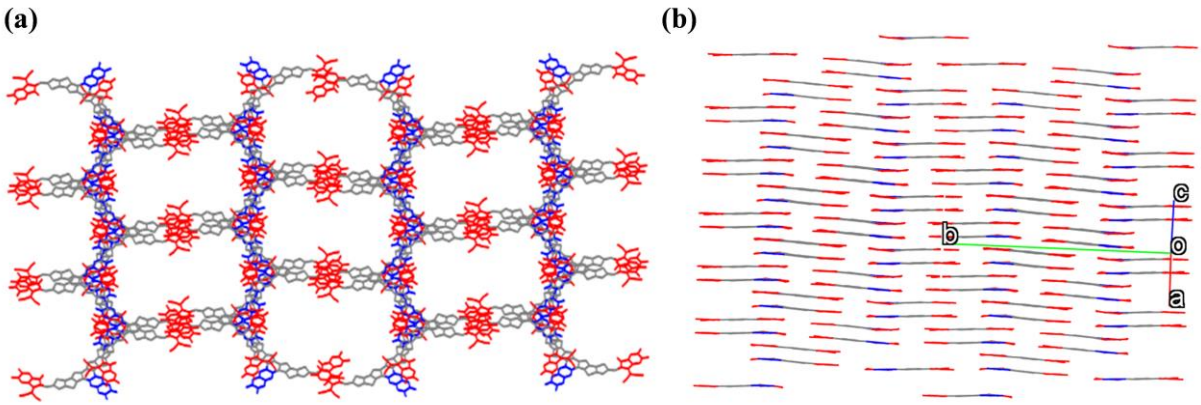

Figure S9. Single-crystal packing diagrams from the (a) top view and (b) side view of CH-6F. The alkyl chains and hydrogen atoms are omitted for clarity.

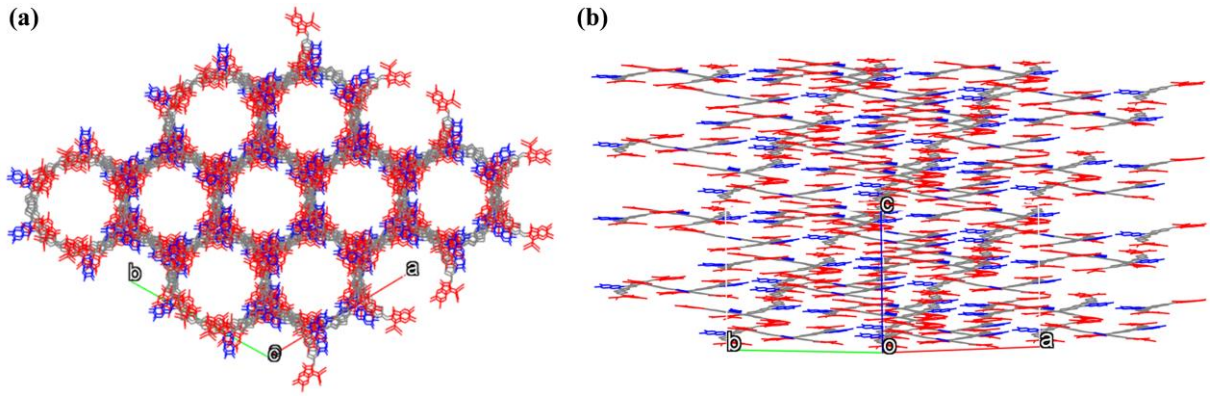

Figure S10. Single-crystal packing diagrams from (a) the top view and (b) side view of CH-4Cl. The alkyl chains and hydrogen atoms are omitted for clarity.

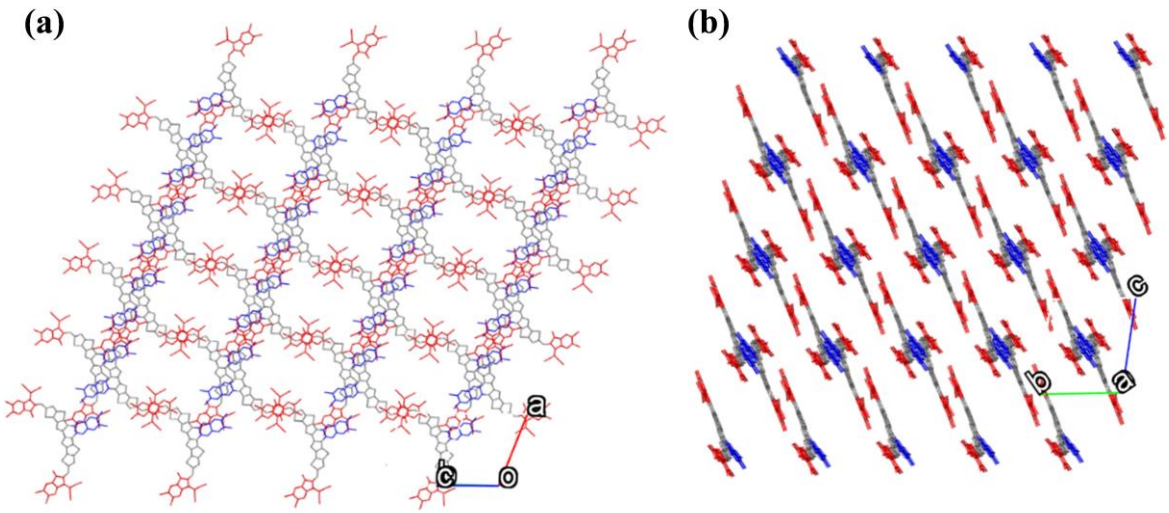

Figure S11. Single-crystal packing diagrams from the (a) the top view and (b) side view of CH-6Cl. The alkyl chains and hydrogen atoms are omitted for clarity.

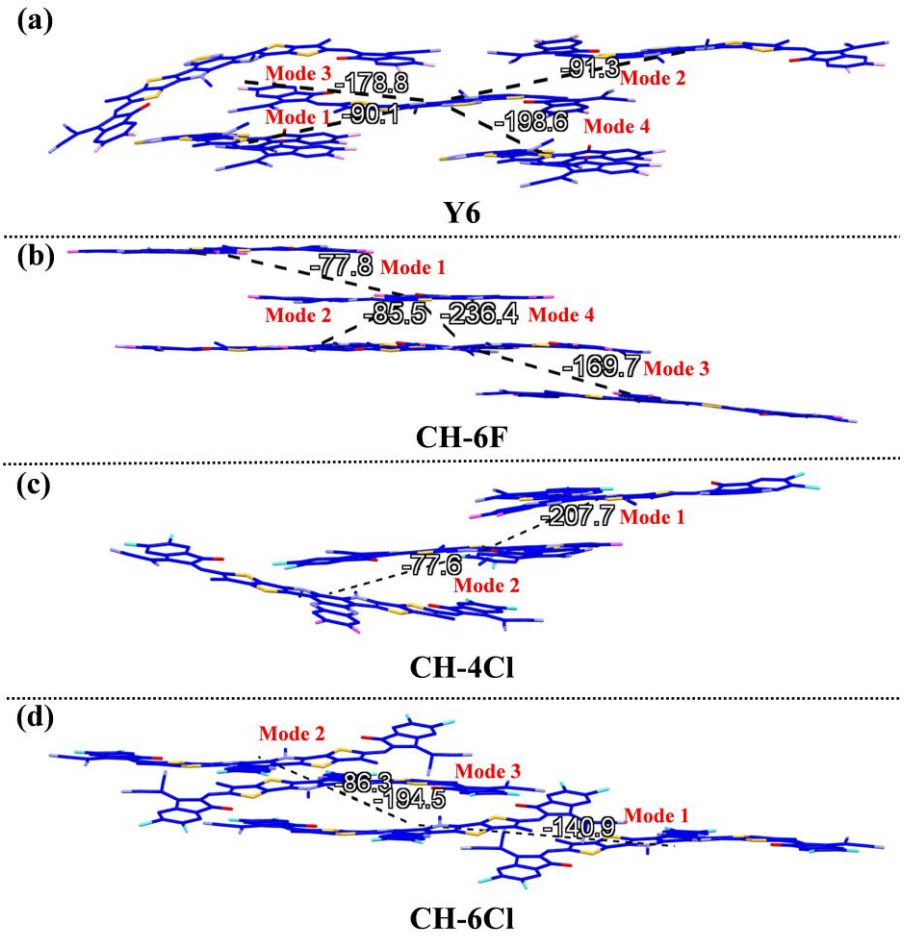

Figure S12. Main UNI inter-molecular potentials (>|70| kJ/mol) and the corresponding defined modes of (a) Y6, (b) CH-6F, (c)CH-4Cl and (d) CH-6Cl with respect to nearest neighbors by Mercury software (kJ/mol). The alkyl chains and hydrogen atoms are omitted for clarity.

Table S1. Crystal data and structure refinement for CH6F, CH-4Cl and CH-6Cl.

Compound		CH-6F	CH-4Cl	CH-6Cl
Empirical formula		$C_{104}H_{120}F_6N_8O_2S_4$	$C_{104}H_{120}Cl_4F_2N_8O_2S_4$	$C_{104}H_{120}Cl_6N_8O_2S_4$
Formula weight		1756.31	1822.11	1855.01
Temperature/k		173.0	173.0	173.0
Crystal system		monoclinic	trigonal	triclinic
Space group		$P2_1/c$	R3c	P-1
Cell	a/Å	17.222(4)	41.303(4)	15.4157(17)
	b/Å	59.388(13)	41.303(4)	17.5066(17)
	c/Å	19.162(5)	32.517(4)	19.617(2)
	α/°	90	90	95.374(6)
	β/°	98.290(12)	90	102.990(7)
	γ/°	90	120	104.699(6)
Volume/Å^3		19394(7)	19394(7)	4925.8(9)
Z		8	8	2
D_{calc}, g/cm^{-3}		1.203	1.203	1.251
μ/mm^{-1}		0.922	0.922	1.844
F(000)		7472.0	7472.0	1964.0
Crystal size/mm^3		0.1×0.1×0.08	0.12×0.11×0.1	0.2×0.1×0.1
Radiation		GaKα (λ=1.34139)	GaKα (λ = 1.34139)	GaKα (λ=1.34139)
2Θ range for data collection/°		4.51 to 102.498	5.194 to 115.318	4.074 to 103.38
Index ranges		$-20 \le h \le 19$, $-68 \le k \le 68$, $-22 \le l \le 22$	$-51 \le h \le 52$, $-51 \le k \le 51$, $-38 \le l \le 40$	$-17 \le h \le 17$, $-20 \le k \le 20$, $-22 \le l \le 22$
Reflections collected		129142	184279	50060
Independent reflections		31826 [R_{int}=0.1461, R_{sigma}=0.1129]	20892 [Rint=0.1077, Rsigma=0.0785]	16305 [R_{int}=0.1432, R_{sigma}=0.1651]
Data/restraints/parameters		31826/1984/2234	20892/733/1119	16305/1042/1193
Goodness-of-fit on F^2		1.029	0.930	1.346
Final R indexes [I>=2σ (I)]		R_1=0.1929, wR_2=0.3973	R_1=0.0932, wR_2=0.2468	R_1=0.1337, wR_2=0.2936
Final R indexes [all data]		R_1=0.2766, wR_2=0.4267	R_1=0.1728, wR_2=0.3145	R_1=0.2840, wR_2=0.3449
Largest diff. peak/hole/e Å^{-3}		0.93/–0.75	0.35/–0.33	1.10/–0.79

The X-ray diffraction signals of single crystals were collected on Rigaku XtalAB PRO MM007 DW at 173.0 K.

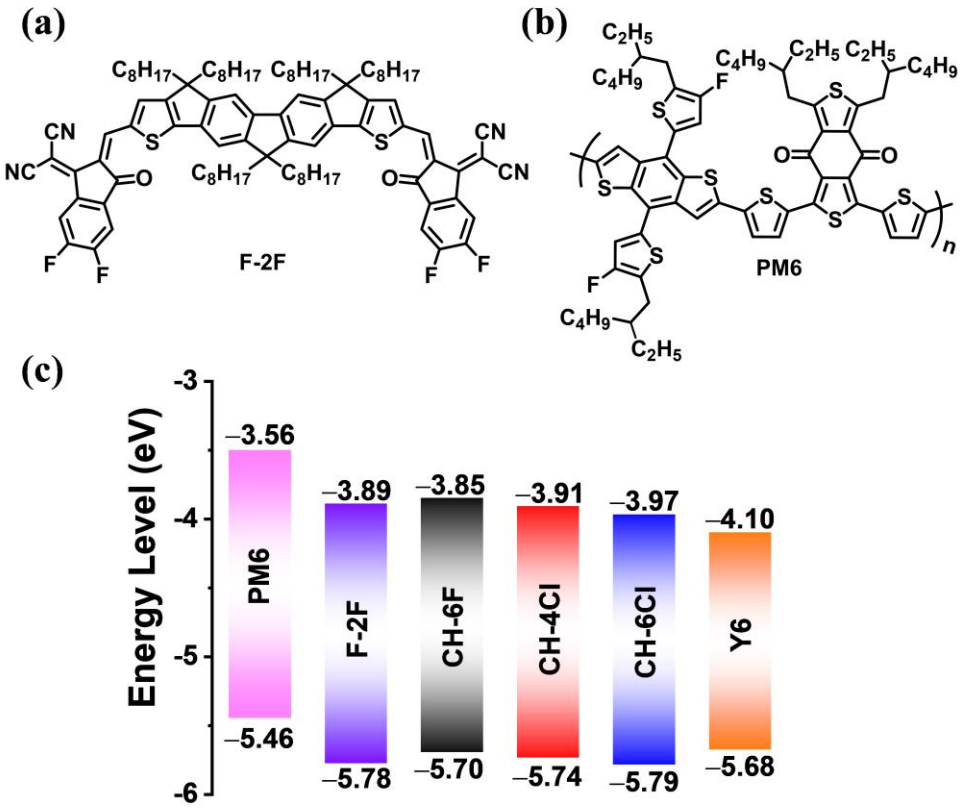

Figure S13. Structures of compound (a) F-2F and (b) PM6, and (c) energy levels of studied chemical materials in this work.

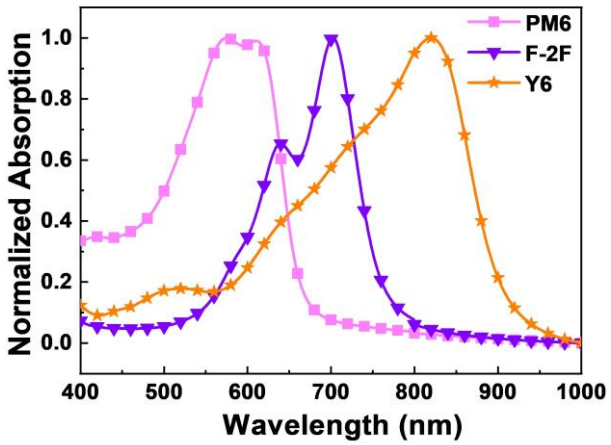

Figure S14. Normalized absorption spectra of PM6, F-2F and Y6 in neat films.

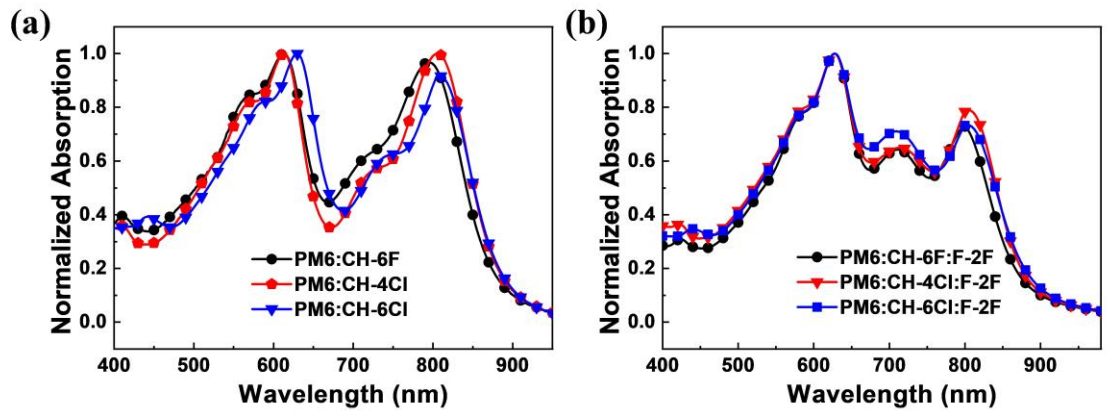

Figure S15. UV-vis absorption spectra of (a) PM6:CH-6F, PM6:CH-4Cl and PM6:CH-6Cl, (b) PM6:CH-6F:F-2F, PM6:CH-4Cl:F-2F and PM6:CH-6Cl:F-2F blend films. The blend films are consistent with optimized devices. The **PM6**:**CH**-series mixtures (D:A=1:1, CF, 14 mg/mL) were spin-casted at 2100 rpm for 30 s onto the PEDOT:PSS layer. The **PM6**:**CH**-series:**F-2F** mixtures (D:A=1:0.9:0.3, CF, 14 mg/mL) were spin-casted at 2200 rpm for 30 s onto the PEDOT:PSS layer. Thermal annealing temperatures are 90℃ or 100℃ for **PM6**:**CH**-series films.

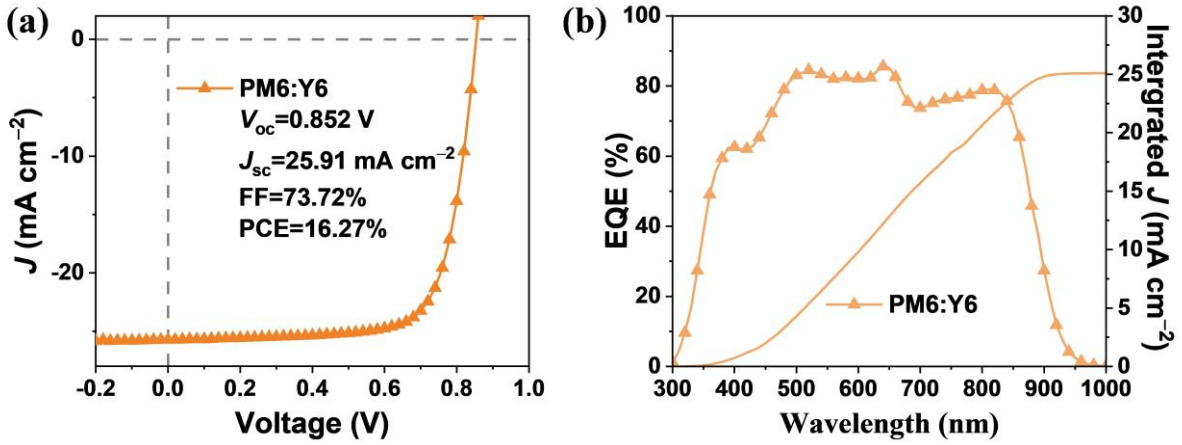

Figure S16. Photovoltaic performance of optimized PM6:Y6. (a) Current density-voltage curves. (b) EQE spectra and integral J_{SC} values. The average parameters were calculated from 15 independent devices in Table 3 and Table S16.

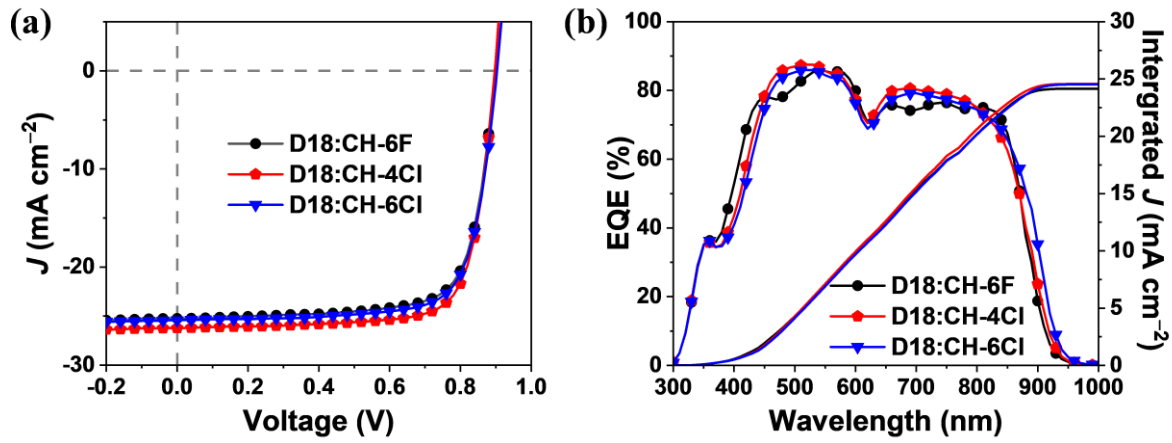

Figure S17. Photovoltaic performance of optimized D18:CH-series. (a) Current density-voltage curves. (b) EQE spectra and integral J_{SC} values. The average parameters were calculated from 15 independent devices in Table S2 and Table S17-19.

Table S2. The optimal photovoltaic parameters of studied OSCs under AM 1.5G Illumination (100 mW cm^{-2}).

Active layer	V_{OC} (V)	[a]J_{SC} (mA cm^{-2})	[b]Calc.J_{SC} (mA/cm^{-2})	[a]FF (%)	[a]PCE (%)
D18:CH-6F	0.897 (0.898±0.003)	25.24 (24.55±0.43)	24.50	74.89 (74.67±0.44)	16.96 (16.45±0.28)
D18:CH-4Cl	0.898 (0.900±0.002)	25.59 (25.29±0.17)	24.91	76.83 (76.27±0.57)	17.65 (17.35±0.13)
D18:CH-6Cl	0.901 (0.898±0.002)	25.42 (25.42±0.25)	24.86	75.10 (74.77±0.55)	17.21 (17.08±0.09)

[a]Optimal and statistical results are listed outside of parentheses and in parentheses, respectively. The average parameters were calculated from 15 independent devices. [b]Current densities calculated from EQE curves.

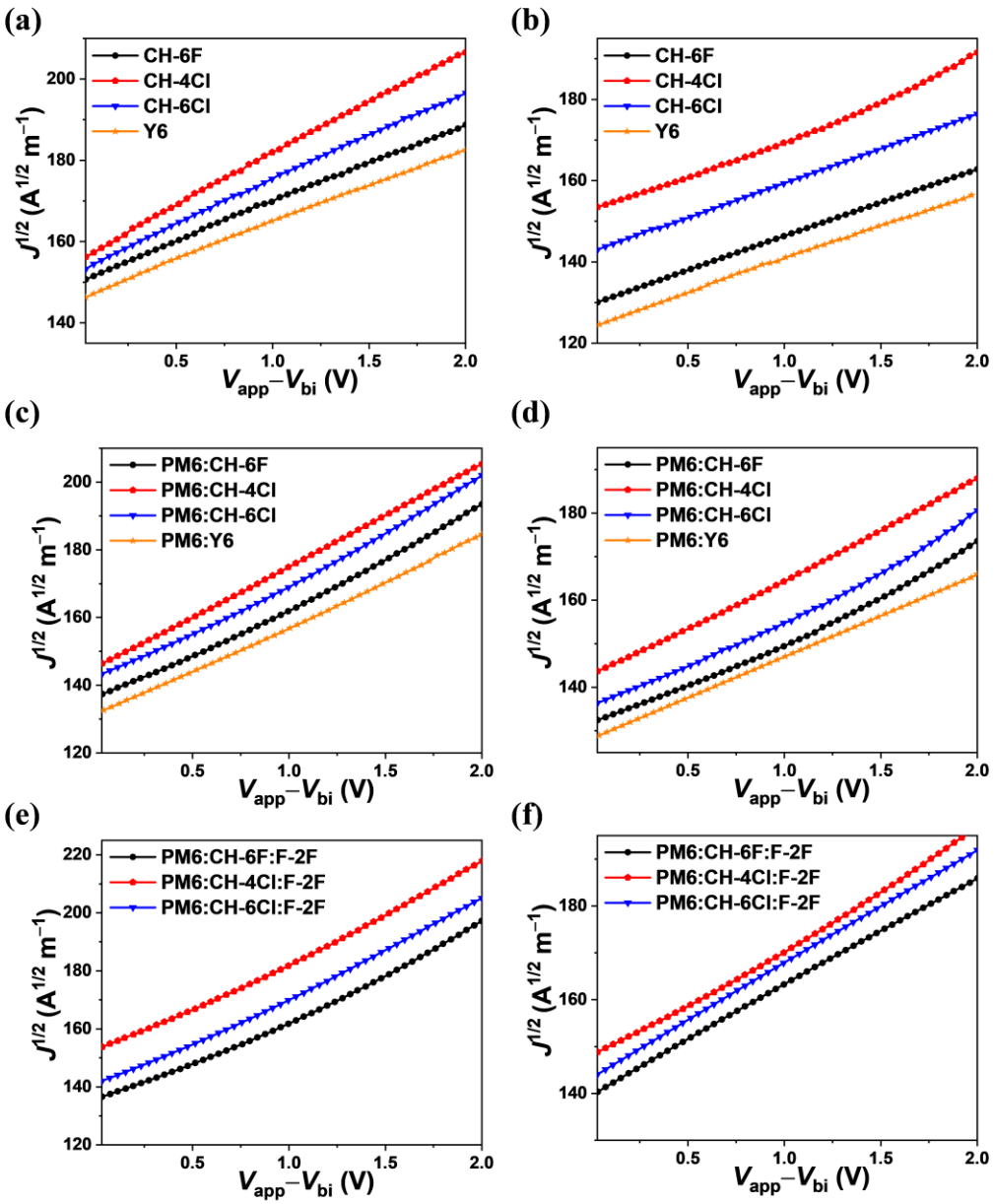

Figure S18. Measurements of electron and hole mobility. SCLC characteristics of **(a)** electron-only and **(b)** hole-only **CH-6F**, **CH-4Cl**, **CH-6Cl** and **Y6** films. **(c)** SCLC characteristics of electron-only devices and **(d)** hole-only devices of **PM6**:**CH-6F**, **PM6**:**CH-4Cl**, **PM6**:**CH-6Cl** and **PM6**:**Y6** blend films. **(e)** SCLC characteristics of electron-only devices and **(d)** hole-only devices of **PM6**:**CH-6F**:**F-2F**, **PM6**:**CH-4Cl**:**F-2F**, and **PM6**:**CH-6Cl**:**F-2F** blend films. The device architectures are ITO/ZnO/active layer/PDNIT-F3N/Al for electron mobility measurements and ITO/PEDOT:PSS/active layer/MoO_3/Al for hole mobility

measurements (the detailed data were shown in **Table S3**). The calculated electron/hole mobility for **PM6**:**CH-6F**:**F-2F**, **PM6**:**CH-4Cl**:**F-2F**, and **PM6**:**CH-6Cl**:**F-2F** are $5.53\times10^{-4}/3.08\times10^{-4}$, $6.17\times10^{-4}/3.55\times10^{-4}$ and $6.05\times10^{-4}/3.39\times10^{-4}$, respectively, with the corresponding μ_e/μ_h ratios of 1.79, 1.74, and 1.78. **PM6**:**CH-4Cl**:**F-2F** based devices exhibit higher and more balanced charge mobilities than that of other ternary devices, which is consistent with the results of binary devices.

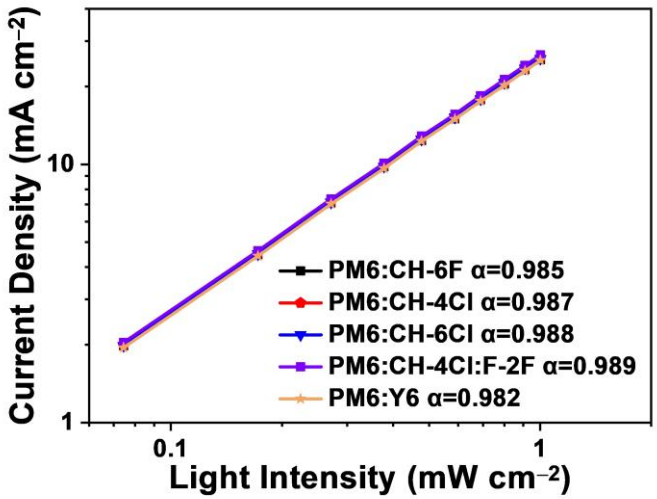

Figure S19. Dependences of J_{SC} on P_{light} of optimized OSCs. The dependences between J_{SC} and P_{light} followed the formula $J_{ph} \propto (P_{light})^{\alpha}$ and the bimolecular recombination is negligible when the α value approaches one.[6] The α values from the **PM6**:**CH-6F**, **PM6**:**CH-4Cl**, **PM6**:**CH-6Cl**, **PM6**:**CH-4Cl**:**F-2F** and **PM6**:**Y6** devices were determined to be 0.985, 0.988, 0.987, 0.989 and 0.982, respectively.

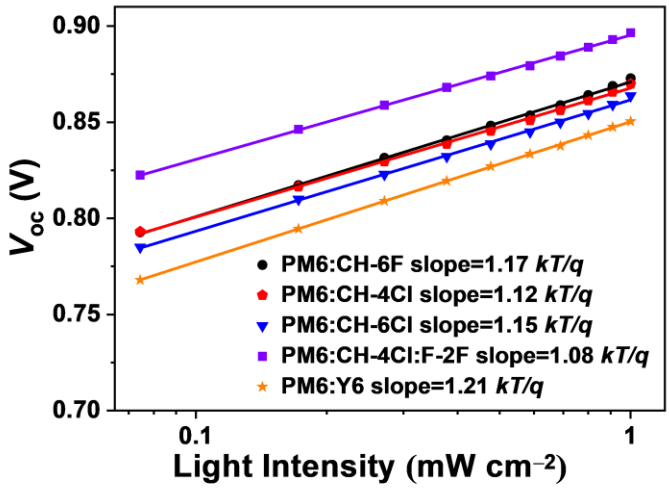

Figure S20. Dependences of V_{OC} on P_{light} of optimized OSCs. Bimolecular recombination is the dominant recombination mechanism when the slope of V_{OC} versus the natural logarithm of P_{light} is equal to kT/q (where k is the Boltzmann constant, T is the Kelvin temperature and q is the elementary charge).[7] The slope values from the **PM6**:**CH-6F**, **PM6**:**CH-4Cl**, **PM6**:**CH-6Cl**, **PM6**:**CH-4Cl**:**F-2F** and **PM6**:**Y6** devices were determined to be 1.17, 1.12, 1.15, 1.08 and 1.21 kT/q, respectively.

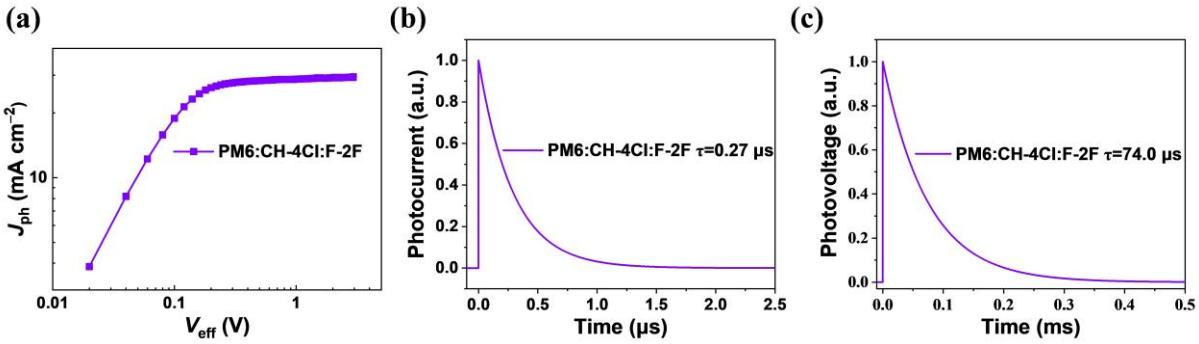

Figure S21. Photovoltaic performances of optimized PM6:**CH-4Cl**:**F-2F. (a) J_{ph} versus V_{eff} curves. (b)Transient photocurrent and (c) transient photovoltage measurements of the devices based on PM6**:**CH-4Cl**:**F-2F.** The exciton dissociation efficiencies (η_{diss}) were obtained using the equation $\eta_{diss}=J_{SC}/J_{sat}$ under short-circuit conditions (J_{sat} is the reverse

saturation current). The charge collection efficiency (η_{coll}) was calculated using the equation $\eta_{coll}=J_{max}/J_{sat}$ (J_{max} is the current density at maximum power). Under the short-circuit conditions, the η_{diss} value is 98.1% for the PM6:CH-4Cl:F-2F and under maximal power output conditions, the η_{coll} value is 88.5%. The PM6:CH-4Cl:F-2F-based device shows a charge sweepout time of 0.27 μs and the carrier lifetime is 74.0 μs.

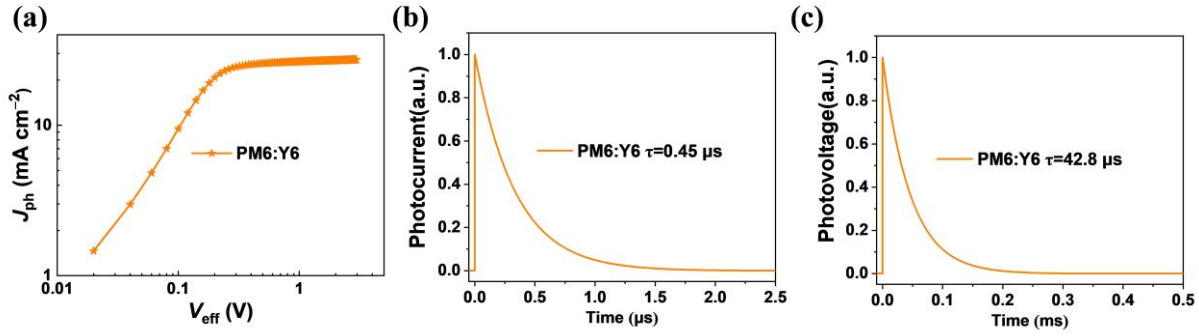

Figure S22. Photovoltaic performances of optimized PM6:Y6. (a) J_{ph} versus V_{eff} curves. (b)Transient photocurrent and (c) transient photovoltage measurements of the devices based on PM6:Y6. Under the short-circuit conditions, the η_{diss} value is 96.8% for the PM6:Y6 and under maximal power output conditions, the η_{coll} value is 86.5%. The PM6:Y6-based device shows a charge sweepout time of 0.45 μs and the carrier lifetime is 42.8 μs.

Table S3. Charge carrier transport parameters of the PM6:CH-6F, PM6:CH-4Cl and PM6:CH-6Cl, PM6:CH-4Cl:F-2F and PM6:Y6 blend and devices.

Blend Films	[a]η_{diss} (%)	[a]η_{coll} (%)	[b]a	[c]Slope (kT/q)	[d]Charge sweepout time (μs)	[d]Carrier lifetimes (μs)	[e]μ_e (10^{-4} cm^2 V^{-1} s^{-1})	[e]μ_h (10^{-4} cm^2 V^{-1} s^{-1})	μ_e/μ_h
PM6:CH-6F	97.8	87.4	0.985	1.17	0.38	45.8	4.69	2.43	1.93
PM6:CH-4Cl	98.0	88.4	0.988	1.12	0.31	68.9	5.24	2.89	1.81
PM6:CH-6Cl	97.9	87.6	0.987	1.15	0.35	58.9	5.10	2.78	1.83
PM6:CH-4Cl:F-2F	98.1	88.5	0.989	1.08	0.27	74.0	6.07	3.43	1.77
PM6:Y6	96.8	86.5	0.982	1.21	0.45	42.8	4.02	2.01	2.00

[a]η_{diss} and η_{coll} were obtained from J_{ph}-V_{eff} pots of optimized OSCs. [b]α was obtained from pots of dependence of current density (J_{SC}) on P_{light} of optimized OSCs. [c]S was the slop of V_{OC} versus the natural logarithm of P_{light} obtained from plots of dependence of V_{OC} on P_{light} of optimized OSCs. [d]The charge sweepout time and carrier lifetimes were calculated from the TPC and TPV measurements, respectively. [e]μ_e and μ_h are electron and hole mobilities of the related blends by SCLC measurements. (All these data are displayed in **Fig. 4e-i** and **Fig. S18-S22**)

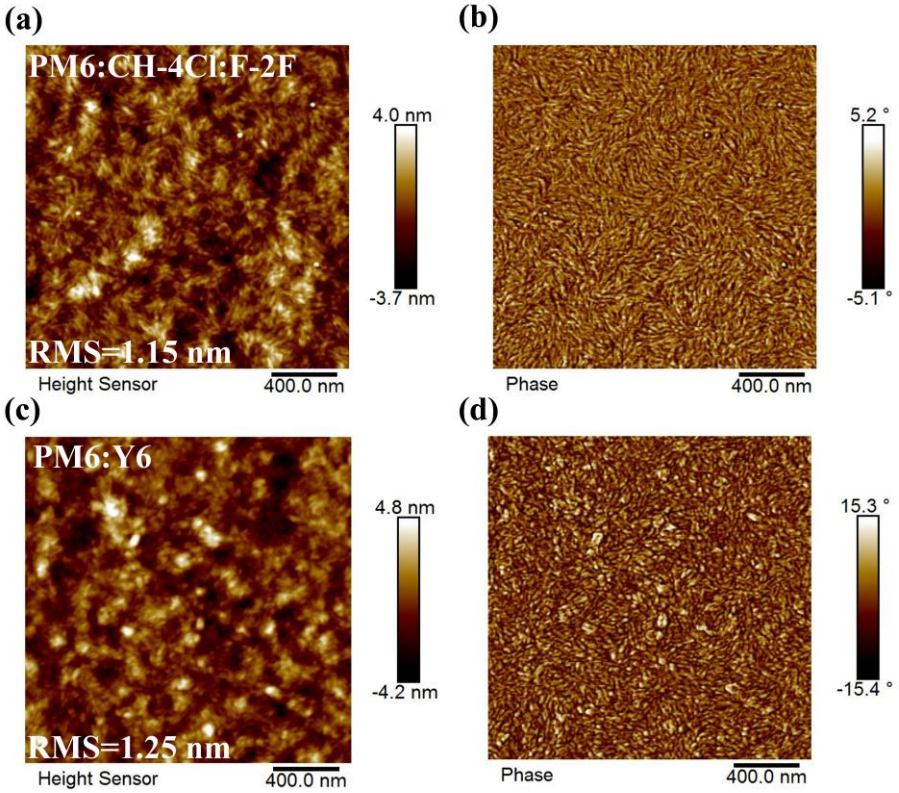

Figure S23. Atomic force microscopy (AFM) for the PM6:**CH-4Cl**:**F-2F and PM6**:**Y6 blend film. (a, b)** AFM height images. **(c, d)** AFM phase images.

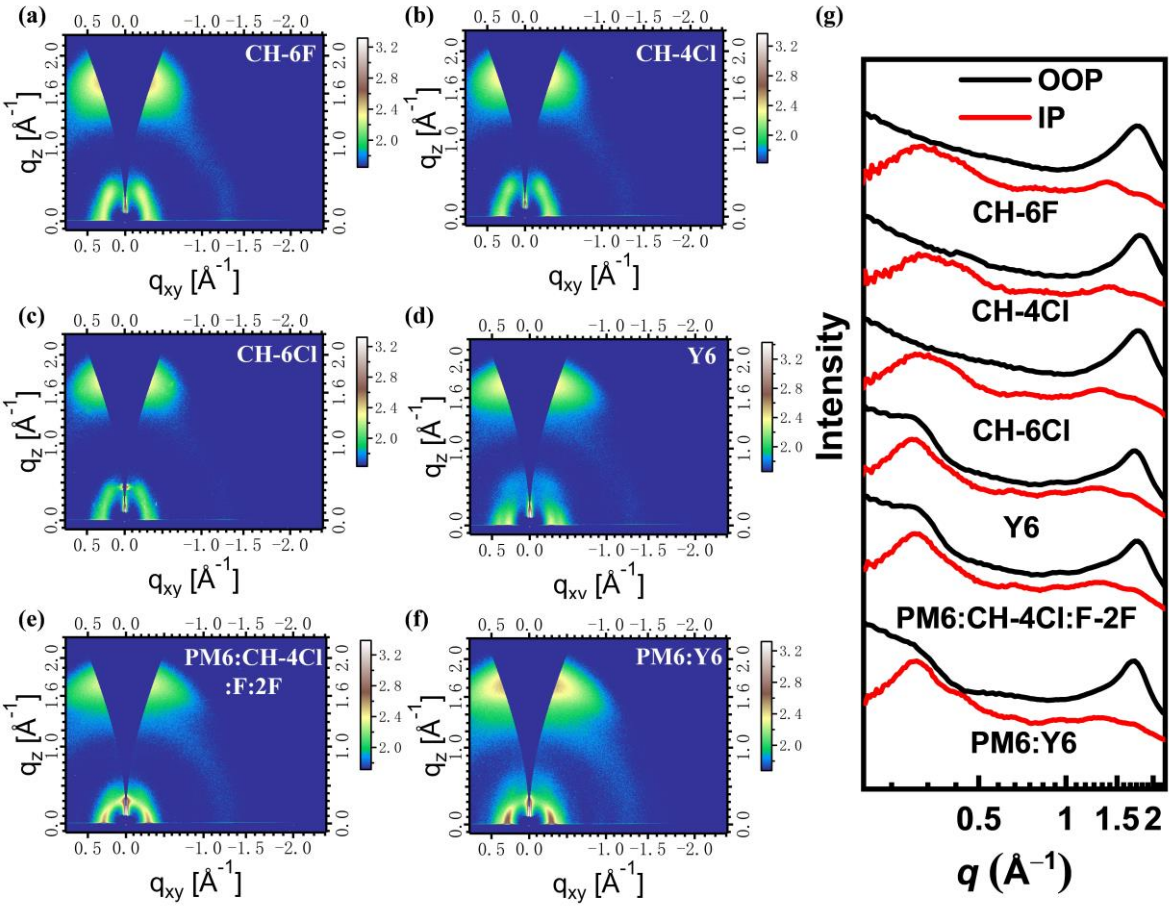

Figure S24. 2D GIWAXS patterns of CH-6F, CH-4Cl, CH-6Cl and Y6 neat films and PM6:CH-4Cl:F-2F and PM6:Y6 blend films and the corresponding IP (black dash line) and OOP (red solid line) extracted line-cut profiles. (a-f) 2D-GIWAXS patterns and (g) 1D line-cuts. The detailed parameters of corresponding 2D GIWAXS were in **Table S4**.

Table S4. The detailed parameters of corresponding 2D GIWAXS.

Materials	(010) peak				(100) peak			
	q (Å^{-1})	[a]*d*-spacing (Å)	FWHM (Å^{-1})	[b]CCL (Å)	*q* (Å^{-1})	[a]*d*-spacing (Å)	FWHM (Å^{-1})	[b]CCL (Å)
CH-6F	1.763	3.564	0.289	19.567	0.310	20.268	0.135	41.888
CH-4Cl	1.792	3.506	0.285	19.842	0.324	19.393	0.129	43.836
CH-6Cl	1.774	3.542	0.270	20.944	0.313	20.074	0.127	44.527
Y6	1.723	3.647	0.290	19.500	0.291	21.592	0.100	56.549
PM6:CH-6F	1.736	3.619	0.309	18.301	0.345	18.212	0.068	83.160

PM6:CH-4Cl	1.752	3.586	0.293	19.300	0.294	21.371	0.063	89.760
PM6:CH-6Cl	1.749	3.592	0.283	19.982	0.291	21.592	0.062	91.208
PM6:Y6	1.705	3.685	0.296	19.104	0.305	20.601	0.077	73.440
PM6:CH-4Cl:F-2F	1.761	3.568	0.292	19.366	0.297	21.156	0.061	92.703

[a]Calculated from the equation: d-spacing=2π/q. [b]Obtained from the Scherrer equation: CCL= 2πK/FWHM, where FWHM is the full-width at half-maximum and K is a shape factor (K= 0.9 here).

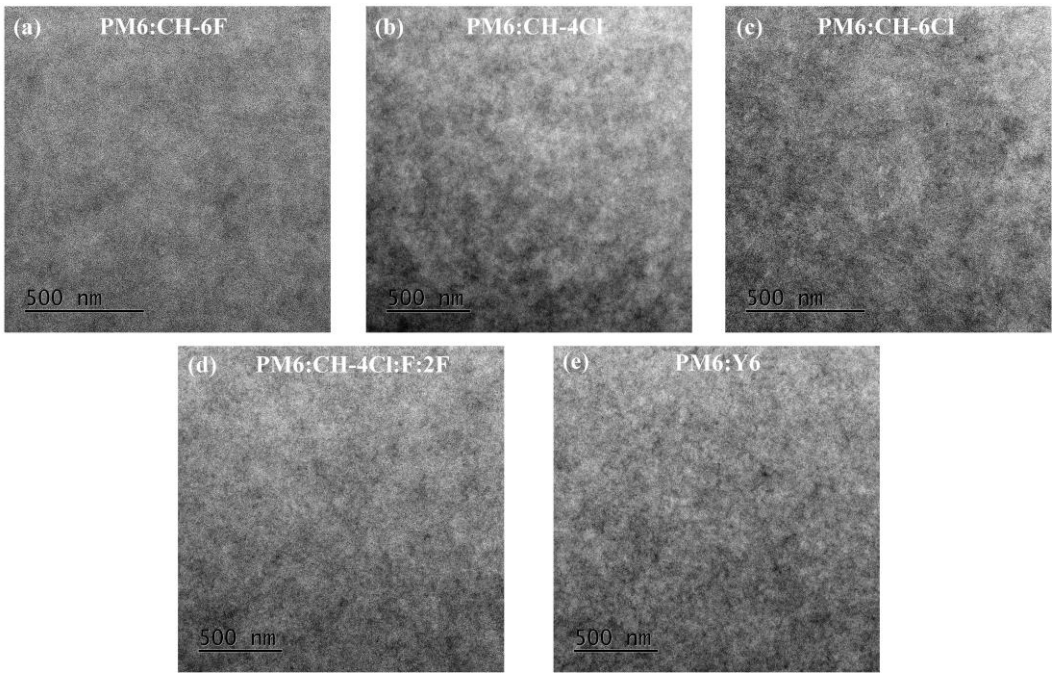

Figure S25. TEM images of optimized (a) PM6:**CH-6F, (b) PM6**:**CH-4Cl, (c) PM6**:**CH-6Cl**, **(d) PM6**:**CH-4Cl**:**F-2F and (e) PM6:Y6 blend films**. The overall morphological characteristics suggested by the TEM images are consistent with corresponding AFM images.

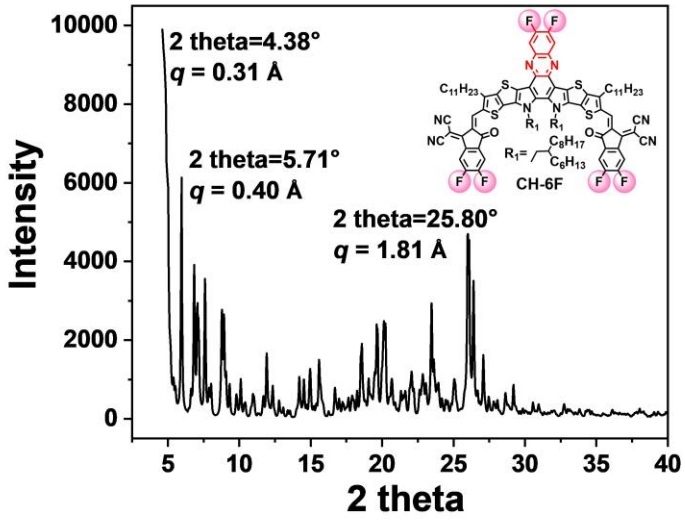

Figure S26. CH-6F X-ray diffraction pattern generated with Mercury CSD software using CH-6F single crystal diffraction data. According to the Bragg equation $2d\sin\theta = \lambda$ and $d = 2\pi/q$, there are strong peaks of 0.31, 0.40 and 1.82 $Å^{-1}$ observed in X-ray diffraction pattern generated from single crystal structure data of **CH-6F**, corresponding to the packing distances of 20.15, 15.46 and 3.45 Å, respectively.

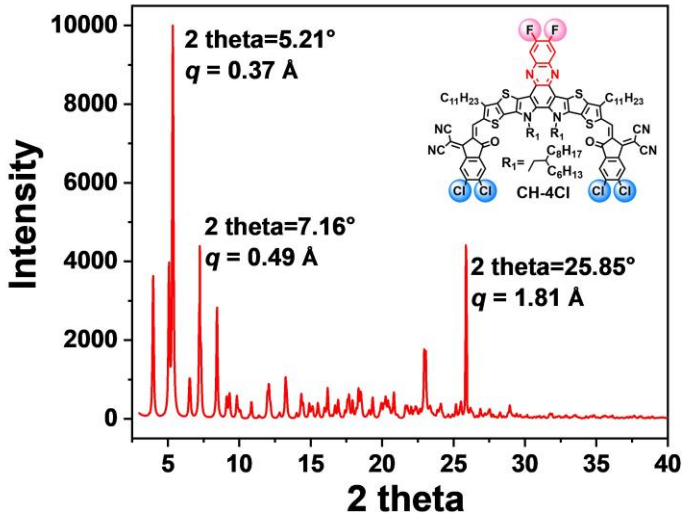

Figure S27. CH-4Cl X-ray diffraction pattern generated with Mercury CSD software using CH-4Cl single crystal diffraction data. According to the Bragg equation $2d\sin\theta = \lambda$ and $d = 2\pi/q$, there are strong peaks of 0.37, 0.49 and 1.81 $Å^{-1}$ observed in X-ray diffraction pattern generated from single crystal structure data of **CH-4Cl**, corresponding to the packing distances of 17.12, 12.33 and 3.44 Å, respectively.

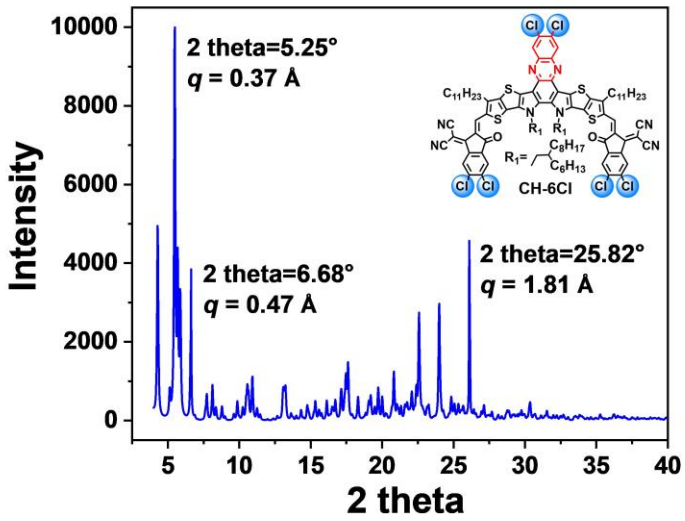

Figure S28. CH-6Cl X-ray diffraction pattern generated with Mercury CSD software using CH-6Cl single crystal diffraction data. According to the Bragg equation $2d\sin\theta = \lambda$ and $d = 2\pi/q$, there are strong peaks of 0.37, 0.47 and 1.81 $Å^{-1}$ observed in X-ray diffraction pattern generated from single crystal structure data of CH17, corresponding to the packing distances of 16.81, 13.22 and 3.44 Å, respectively.

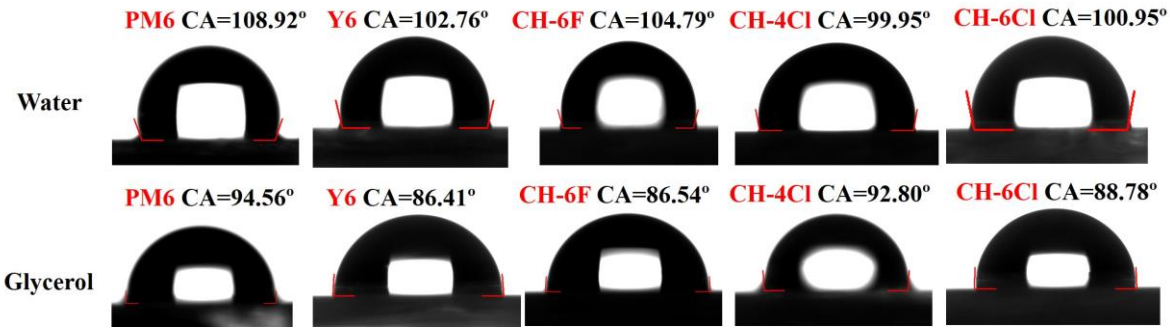

Figure S29. The images of water and glycerol drops on **PM6**, **CH-6F**, **CH-4Cl**, **CH-6Cl** and **Y6** pure films.

Table S5. The detailed parameters about surface energies of **PM6**, **CH-6F**, **CH-4Cl**, **CH-6Cl** and **Y6** pure films.

	γ_S^d (mN m^{-1})	γ_S^p (mN m^{-1})	$^a\gamma_{SV}$ (mN m^{-1})	$^b\chi_{pm6:A}$ (K)
PM6	0.82	16.27	17.09	–
CH-6F	1.33	20.71	22.04	0.31
CH-4Cl	0.24	20.61	20.85	0.19
CH-6Cl	0.63	21.62	22.25	0.34
Y6	1.09	21.67	22.76	0.40

$^a\gamma_{SV}$ represents the interfacial surface energy between compound **PM6** and different acceptors. $^b\chi_{pm6:A}$ represents the Flory-Huggins interaction parameter between compound **PM6** and compound A (or blend A).

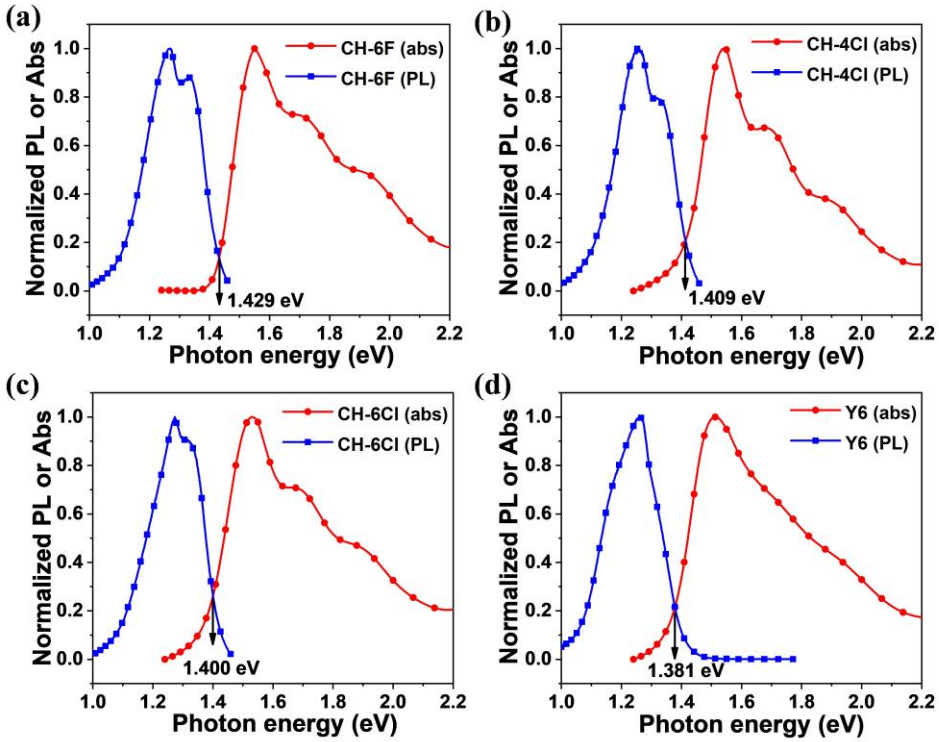

Figure S30. Details of optical E_g determination for (a) CH-6F, (b) CH-4Cl, (c) CH-6Cl and (d) Y6. E_g is estimated by the cross-point of normalized absorption (red lines) and photoluminescence (PL) spectra (blue lines)[8] of the **CH-6F**, **CH-4Cl**, **CH-6Cl** and **Y6** neat films at 1.429, 1.409, 1.400 and 1.381 eV, respectively.

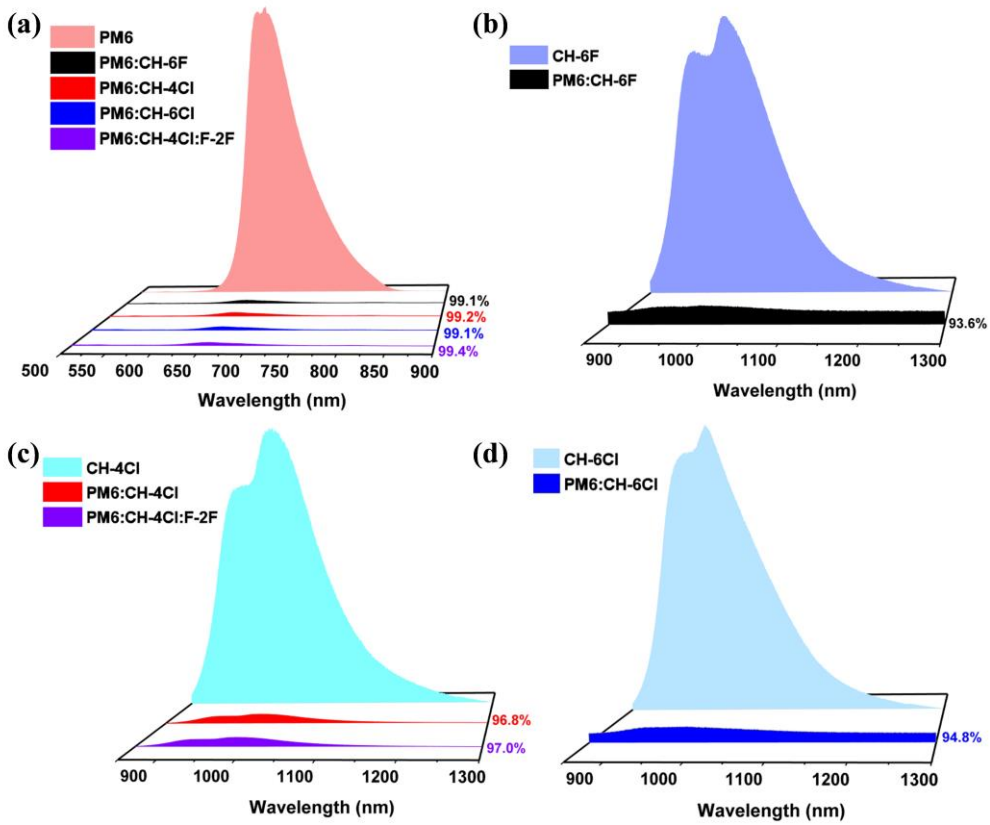

Figure S31. Photoluminescence curves of the PM6 excited at 460 nm and CH-6F, CH-4Cl and CH-6Cl neat films excited at 826 nm. (a) Fluorescence quenching efficiency of **PM6**:**CH-6F**, **PM6**:**CH-4Cl**, **PM6**:**CH-6Cl**, **PM6**:**CH-4Cl**:**F-2F** and **PM6**:**Y6** blend films excited at 460 nm. Fluorescence quenching efficiency of **(b) PM6**:**CH-6F, (c) PM6**:**CH-4Cl** and **PM6**:**CH-4Cl**:**F-2F**, **(d) PM6**:**CH-6Cl** blend films excited at 826 nm.

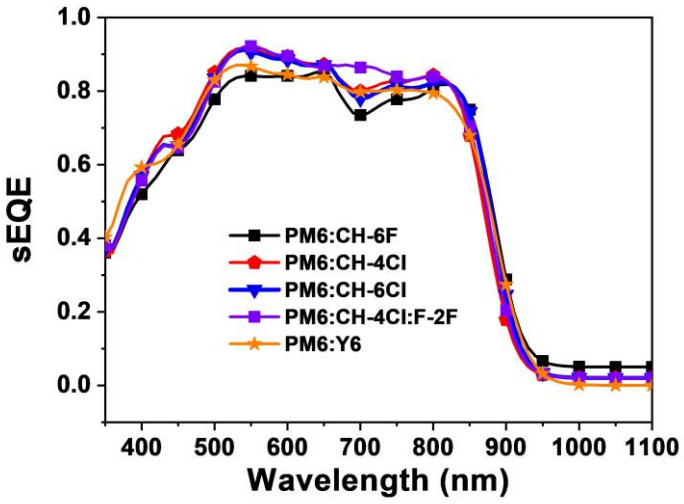

Figure S32. sEQE of PM6:CH-6F, PM6:CH-4Cl, PM6:CH-6Cl, PM6:CH-4Cl:F-2F and PM6:Y6 based OSCs.

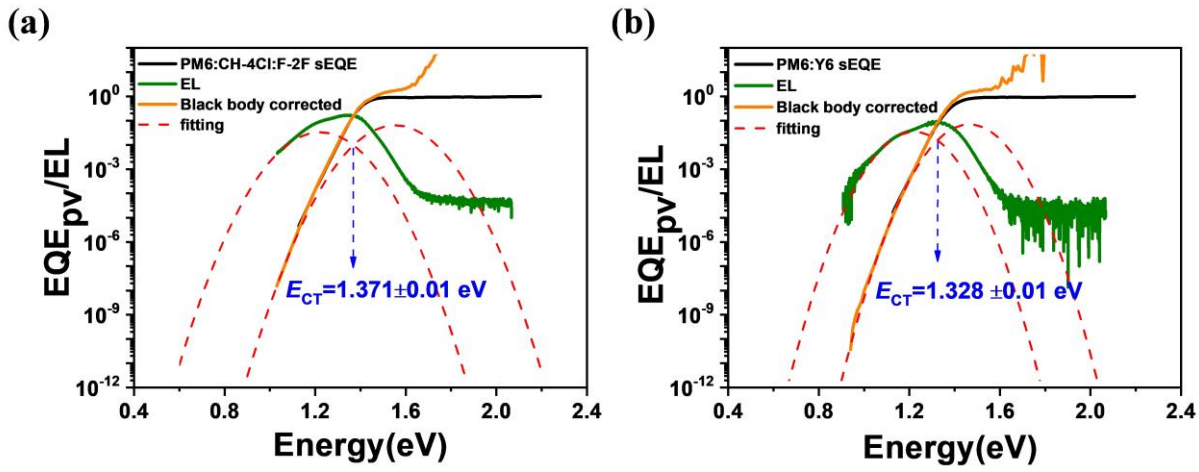

Figure S33. sEQE spectra and the fitting results for PM6:CH-4Cl:F-2F and PM6:Y6 based device.

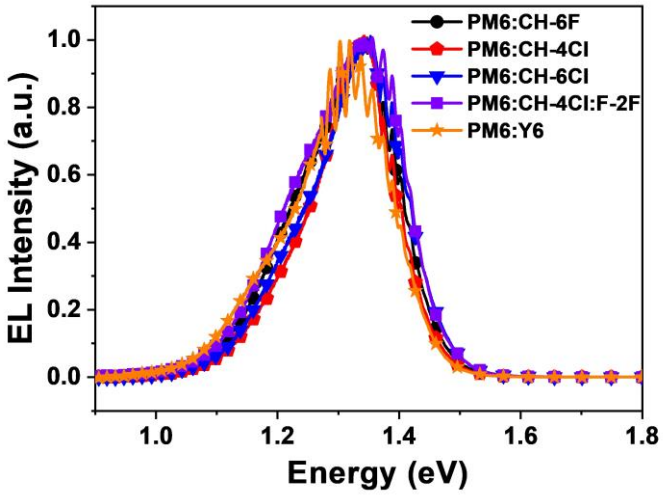

Figure S34. Normalized electroluminescence spectra (EL) curves of PM6:CH-6F, PM6:CH-4Cl, PM6:CH-6Cl, PM6:CH-4Cl:F-2F and PM6:Y6 based OSCs.

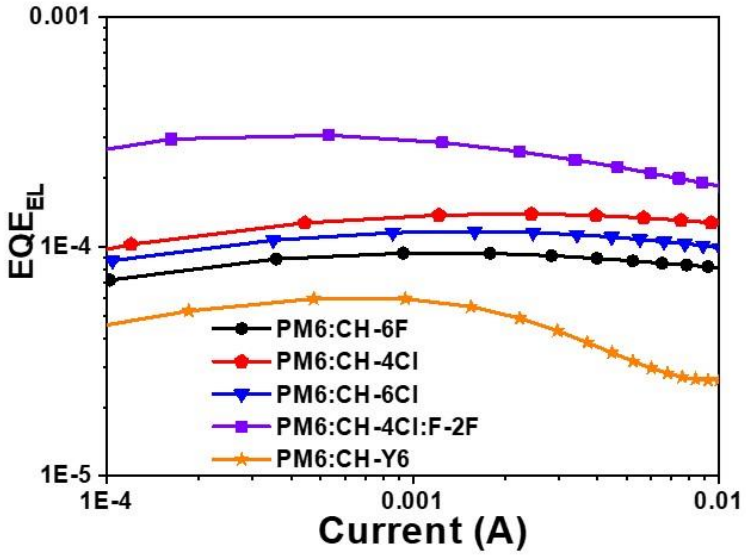

Figure S35. EQE$_{EL}$ spectra of PM6:CH-6F, PM6:CH-4Cl, PM6:CH-6Cl, PM6:CH-4Cl:F-2F and PM6:Y6 based OSCs.

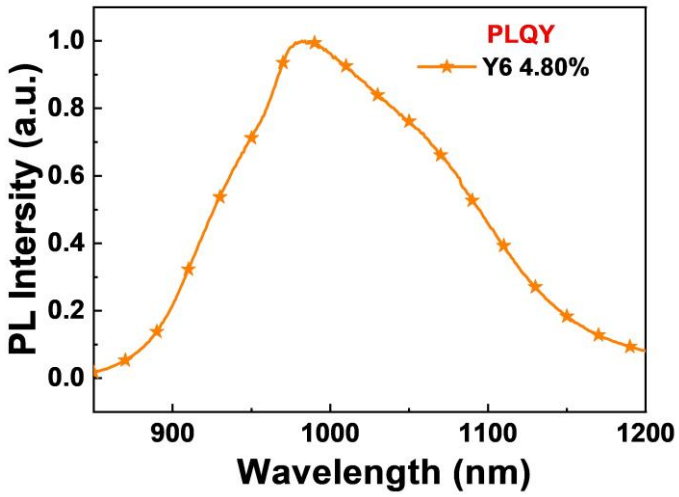

Figure S36. Photoluminescence spectra of the Y6 film excited at 826 nm together with their quantum efficiencies.

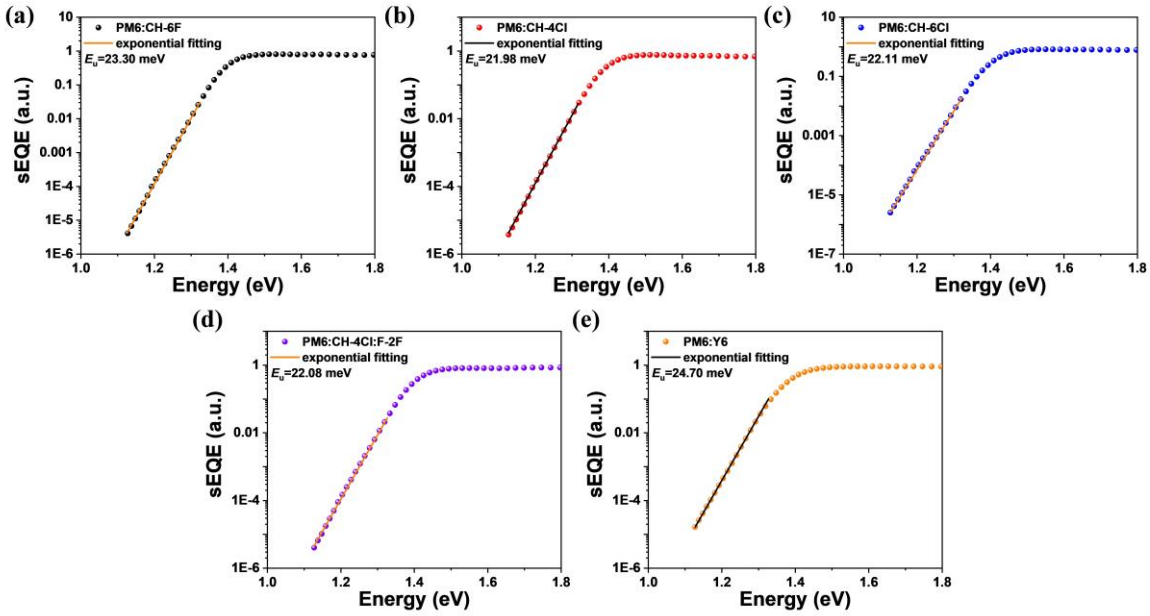

Figure S37. Sensitive external quantum efficiency spectra (sEQE), analysis of energetic disorder of optimized (a) PM6:CH-6F, (b) PM6:CH-4Cl, (c) PM6:CH-6Cl and (d) PM6:CH-4Cl:F-2F OSCs (e) PM6:Y6 at the absorption onset.

Table S6. Detailed photovoltaic parameters of the PM6:CH-6F based devices processed by varied conditions under the illumination of AM 1.5 G, 100 mW cm^{-2}.[a]

D/A (*w*/*w*)	CN (*v*/*v*)	TA (°C)	V_{OC} (V)	J_{SC} (mA cm^{-2})	FF (%)	PCE (%)
1:0.8	-	-	0.906	22.86	69.97	14.49
1:1	-	-	0.903	24.88	70.53	15.84
1:1.2	-	-	0.898	24.87	68.62	15.32
1:1	-	80	0.890	24.30	71.26	15.41
	-	90	0.889	25.16	71.21	15.92
	-	100	0.886	25.34	71.24	16.00
1:1	0.2%	100	0.874	25.12	73.29	16.09
	0.3%	**100**	**0.872**	**25.31**	**75.99**	**16.77**
	0.5%	100	0.866	25.69	74.67	16.61
	0.7%	100	0.854	21.52	72.96	13.41

[a]The device architecture is ITO/PEDOT:PSS/active layer/PNDIT-F3N/Ag, D=14 mg/mL in chloroform, the resulting active layer solutions were spin-casted at 2100 rpm for 30 s.

Table S7. Detailed photovoltaic parameters of the PM6:CH-4Cl based devices processed by varied conditions under the illumination of AM 1.5 G, 100 mW cm^{-2}.[a]

D/A (*w*/*w*)	CN (*v*/*v*)	TA (°C)	V_{OC} (V)	J_{SC} (mA cm^{-2})	FF (%)	PCE (%)
1:0.8	-	-	0.893	23.34	68.42	14.26
1:1	-	-	0.890	24.53	70.50	15.39
1:1.2	-	-	0.886	23.28	66.76	13.77
1:1	-	80	0.885	24.55	70.53	15.32
	-	90	0.876	24.54	71.99	15.47
	-	100	0.871	24.35	66.94	14.20
1:1	0.2%	90	0.873	26.22	74.12	16.97
	0.3%	**90**	**0.872**	**26.50**	**76.68**	**17.72**
	0.5%	90	0.865	26.11	75.74	17.11
	0.7%	90	0.855	22.58	73.51	14.19

[a]The device architecture is ITO/PEDOT:PSS/active layer/PNDIT-F3N/Ag, D=14 mg/mL in chloroform, the resulting active layer solutions were spin-casted at 2100 rpm for 30 s.

Table S8. Detailed photovoltaic parameters of the PM6:CH-6Cl based devices processed by varied conditions under the illumination of AM 1.5 G, 100 mW cm^{-2}.[a]

D/A (*w*/*w*)	CN (*v*/*v*)	TA (°C)	V_{OC} (V)	J_{SC} (mA cm^{-2})	FF (%)	PCE (%)
1:0.8	-	-	0.894	23.14	71.17	14.72
1:1	-	-	0.889	24.51	71.83	15.65
1:1.2	-	-	0.886	24.66	70.82	15.47
1:1	-	80	0.883	24.29	72.39	15.52
	-	90	0.878	24.80	72.89	15.87
	-	100	0.876	24.93	72.02	15.72
1:1	0.2%	90	0.874	25.76	74.63	16.80
	0.3%	**90**	**0.866**	**26.07**	**76.28**	**17.22**
	0.5%	90	0.863	25.70	75.43	16.64
	0.7%	90	0.845	23.68	73.58	14.72

[a]The device architecture is ITO/PEDOT:PSS/active layer/PNDIT-F3N/Ag, D=14 mg/mL in chloroform, the resulting active layer solutions were spin-casted at 2100 rpm for 30 s.

Table S9. Detailed photovoltaic parameters of the PM6:CH-4Cl:F-2F based devices processed by varied conditions under the illumination of AM 1.5 G, 100 mW cm^{-2}.[a]

D/A (*w*/*w*)	CN (*v*/*v*)	TA (°C)	V_{OC} (V)	J_{SC} (mA cm^{-2})	FF (%)	PCE (%)
1:1:0.1	0.3%	80	0.879	24.78	74.41	16.21
		90	0.876	26.50	74.55	17.31
		100	0.874	25.86	75.76	17.12

1:1:0.2	0.3%	80	0.887	25.17	75.60	16.88
		90	0.881	26.29	75.76	17.54
		100	0.882	25.57	74.31	16.76
1:1:0.3	0.3%	80	0.885	26.00	70.47	16.21
		90	0.884	26.79	68.86	16.30
		100	0.883	26.86	68.95	16.35
1:0.9:0.1	0.3%	80	0.885	26.40	74.67	17.44
		90	0.882	26.52	73.27	17.13
		100	0.879	26.69	74.01	17.36
1:0.9:0.2	0.3%	80	0.888	26.89	75.00	17.91
		90	0.886	26.19	75.70	17.57
		100	0.877	26.93	74.46	17.55
1:0.9:0.3	**0.3%**	80	0.898	26.29	75.25	17.77
		90	**0.896**	**26.69**	**76.17**	**18.22**
		100	0.889	26.72	75.75	17.99
1:0.9:0.4	0.3%	80	0.894	26.21	72.86	17.07
		90	0.889	26.78	72.27	17.21
		100	0.883	26.28	71.91	16.69

[a]The device architecture is ITO/PEDOT:PSS/active layer/PNDIT-F3N/Ag, D=14 mg/mL in chloroform, the resulting active layer solutions were spin-casted at 2100 rpm for 30 s.

Table S10. Detailed photovoltaic parameters of the PM6:CH-6F based devices by optimal conditions under the illumination of AM 1.5 G, 100 mW cm^{-2}.[a]

Active layer	V_{OC} (V)	J_{SC} (mA cm^{-2})	FF (%)	PCE (%)
PM6:CH-6F	0.872	25.30	75.09	16.57
	0.873	25.63	74.87	16.75
	0.873	25.21	75.11	16.53
	0.877	24.76	75.96	16.49
	0.875	24.62	75.83	16.34
	0.874	24.68	75.71	16.38
	0.874	25.00	74.96	16.33
	0.877	25.49	74.50	16.65
	0.875	25.45	75.03	16.71
	0.874	25.14	75.41	16.57
	0.872	**25.31**	**75.99**	**16.77**
	0.869	25.56	75.54	16.78
	0.874	24.88	76.41	16.62
	0.874	24.55	77.24	16.57
	0.872	25.30	75.09	16.57
[b]Average	**0.874**	**25.13**	**75.52**	**16.58**

[a]The device architecture is ITO/PEDOT:PSS/active layer/PNDIT-F3N/Ag, D=14 mg/mL in chloroform with 0.3 vol% CN, the resulting active layer solutions were spin-casted at 2100 rpm for 30 s; TA (100 °C). [b]The average values are obtained from 15 devices.

Table S11. Detailed photovoltaic parameters of the PM6:CH-4Cl based devices by optimal conditions under the illumination of AM 1.5 G, 100 mW cm^{-2}.[a]

Active layer	V_{OC} (V)	J_{SC} (mA cm^{-2})	FF (%)	PCE (%)
	0.874	26.46	76.54	17.70
	0.871	26.50	76.13	17.57
	0.871	26.28	75.86	17.36
	0.870	26.61	75.56	17.49
	0.869	26.63	75.53	17.48
	0.872	26.39	76.04	17.50
	0.872	26.43	75.67	17.44
PM6:CH-4Cl	0.871	26.63	75.83	17.59
	0.873	26.33	75.84	17.43
	0.872	**26.50**	**76.68**	**17.72**
	0.871	26.23	76.45	17.47
	0.870	26.73	75.59	17.58
	0.871	26.83	75.30	17.60
	0.871	26.53	76.40	17.65
	0.870	26.43	75.67	17.40
[b]Average	**0.871**	**26.49**	**75.94**	**17.53**

[a]The device architecture is ITO/PEDOT:PSS/active layer/PNDIT-F3N/Ag, D=14 mg/mL in chloroform with 0.3 vol% CN, the resulting active layer solutions were spin-casted at 2100 rpm for 30 s; TA (90 °C). [b]The average values are obtained from 15 devices.

Table S12. Detailed photovoltaic parameters of the PM6:CH-6Cl based devices by optimal conditions under the illumination of AM 1.5 G, 100 mW cm^{-2}.[a]

Active layer	V_{OC} (V)	J_{SC} (mA cm^{-2})	FF (%)	PCE (%)
	0.864	26.20	75.35	17.06
	0.864	26.13	75.05	16.94
	0.865	26.05	74.52	16.79
	0.871	25.82	74.56	16.77
	0.868	25.78	75.33	16.86
	0.867	25.90	75.79	17.02
	0.867	25.85	76.08	17.05
PM6:CH-6Cl	0.865	25.95	76.22	17.11
	0.863	26.13	75.97	17.13
	0.859	25.83	76.09	16.88
	0.866	**26.07**	**76.28**	**17.22**
	0.865	26.20	75.75	17.17
	0.865	26.12	75.24	17.00
	0.865	26.21	74.83	16.97
	0.864	26.20	75.35	17.06
[b]Average	**0.865**	**26.03**	**75.49**	**17.00**

[a]The device architecture is ITO/PEDOT:PSS/active layer/PNDIT-F3N/Ag, D=14 mg/mL in

chloroform with 0.3 vol% CN, the resulting active layer solutions were spin-casted at 2100 rpm for 30 s; TA (90 °C). [b]The average values are obtained from 15 devices.

Table S13. Detailed photovoltaic parameters of the PM6:CH-6F:F-2F based devices by optimal conditions under the illumination of AM 1.5 G, 100 mW cm^{-2}.[a]

Active layer	V_{OC} (V)	J_{SC} (mA cm^{-2})	FF (%)	PCE (%)
PM6:CH-6F:F-2F	0.898	26.13	73.09	17.15
	0.900	**25.69**	**74.48**	**17.22**
	0.898	25.89	73.13	17.00
	0.898	25.84	73.29	17.01
	0.902	25.84	73.75	17.19
	0.899	26.03	73.37	17.17
	0.898	25.73	73.21	16.92
	0.895	25.81	73.30	16.93
	0.895	25.62	74.61	17.11
	0.894	25.60	74.72	17.10
	0.897	25.60	74.61	17.13
	0.895	25.57	74.56	17.06
	0.897	25.66	74.32	17.11
	0.896	25.87	73.69	17.08
	0.899	25.53	74.58	17.12
[b]Average	**0.897**	**25.76**	**73.91**	**17.09**

[a]The device architecture is ITO/PEDOT:PSS/active layer/PNDIT-F3N/Ag; D=14 mg/mL in chloroform with 0.5 vol% CN; the resulting active layer solutions were spin-casted at 2200 rpm for 30 s; TA (90 °C). [b]The average values are obtained from 15 devices.

Table S14. Detailed photovoltaic parameters of the PM6:CH-4Cl:F-2F based devices by optimal conditions under the illumination of AM 1.5 G, 100 mW cm^{-2}.[a]

Active layer	V_{OC} (V)	J_{SC} (mA cm^{-2})	FF (%)	PCE (%)
PM6:CH-4Cl:F-2F	0.892	26.34	75.83	17.82
	0.894	26.54	75.93	18.02
	0.894	26.71	75.98	18.14
	0.893	26.51	75.37	17.84
	0.897	26.51	75.02	17.84
	0.896	26.43	76.26	18.06
	0.899	25.91	76.83	17.90
	0.893	26.46	76.14	17.99
	0.885	26.65	76.41	18.02
	0.896	**26.69**	**76.17**	**18.22**
	0.895	26.55	76.03	18.07
	0.896	26.57	76.03	18.10
	0.893	26.69	76.06	18.13

	0.893	26.66	75.84	18.06
	0.892	26.35	75.99	17.86
[b]Average	**0.894**	**26.50**	**75.99**	**18.00**

[a]The device architecture is ITO/PEDOT:PSS/active layer/PNDIT-F3N/Ag; D=14 mg/mL in chloroform with 0.5 vol% CN; the resulting active layer solutions were spin-casted at 2200 rpm for 30 s; TA (90 °C). [b] The average values are obtained from 15 devices.

Table S15. Detailed photovoltaic parameters of the PM6:CH-6Cl:F-2F based devices by optimal conditions under the illumination of AM 1.5 G, 100 mW cm^{-2}.[a]

Active layer	V_{OC} (V)	J_{SC} (mA cm^{-2})	FF (%)	PCE (%)
	0.889	26.15	74.23	17.26
	0.890	25.98	74.73	17.28
	0.892	26.27	74.56	17.47
	0.891	25.96	74.85	17.31
	0.889	25.97	75.30	17.39
	0.889	25.97	75.30	17.38
	0.892	25.79	75.33	17.32
PM6:CH-6Cl:F-2F	**0.892**	**26.34**	**74.79**	**17.57**
	0.892	26.33	74.56	17.52
	0.890	26.18	74.27	17.31
	0.888	26.17	75.30	17.50
	0.888	25.82	75.23	17.24
	0.890	26.04	74.88	17.36
	0.889	26.06	75.12	17.40
	0.888	26.20	74.55	17.35
[b]Average	**0.890**	**26.08**	**74.87**	**17.38**

[a]The device architecture is ITO/PEDOT:PSS/active layer/PNDIT-F3N/Ag; D=14 mg/mL in chloroform with 0.5 vol% CN; the resulting active layer solutions were spin-casted at 2200 rpm for 30 s; TA (90 °C). [b] The average values are obtained from 15 devices.

Table S16. Detailed photovoltaic parameters of the PM6:Y6 based devices by optimal conditions under the illumination of AM 1.5 G, 100 mW cm^{-2}.[a]

Active layer	V_{OC} (V)	J_{SC} (mA cm^{-2})	FF (%)	PCE (%)
	0.852	**25.91**	**73.72**	**16.27**
	0.847	26.15	73.11	16.19
	0.846	26.09	73.35	16.19
	0.854	25.5	74.06	16.13
PM6:Y6	0.853	25.51	73.83	16.07
	0.852	25.41	73.27	15.86
	0.849	25.57	73.87	16.04
	0.854	25.5	74.06	16.13
	0.851	26.12	72.98	16.22

	0.847	25.84	73.73	16.14
	0.850	25.84	72.08	15.83
	0.851	25.81	73.89	16.23
	0.850	25.83	72.73	15.97
	0.851	26.09	71.41	15.85
	0.848	26.14	73.23	16.23
[b]Average	**0.850**	**25.82**	**73.29**	**16.09**

[a]The device architecture is ITO/PEDOT:PSS/active layer/PDINO/Ag; D=12 mg/mL in chloroform with 0.5 vol% CN; the resulting solutions were spin-casted at 2200 rpm for 30 s onto the PEDOT:PSS layer; TA (100 ℃). [b] The average values are obtained from 15 devices.

Table S17. Detailed photovoltaic parameters of the D18:CH-6F based devices by optimal conditions under the illumination of AM 1.5 G, 100 mW cm^{-2}.[a]

Active layer	V_{OC} (V)	J_{SC} (mA cm^{-2})	FF (%)	PCE (%)
	0.898	24.71	75.13	16.67
	0.900	25.14	74.19	16.79
	0.895	24.08	74.86	16.13
	0.898	24.15	75.38	16.35
	0.894	24.18	74.62	16.13
	0.891	24.26	74.66	16.15
	0.901	24.05	74.94	16.25
D18:CH-6F	0.900	24.76	73.64	16.40
	0.899	25.20	74.40	16.86
	0.899	24.93	74.02	16.58
	0.899	24.35	74.74	16.35
	0.898	24.81	75.13	16.74
	0.897	**25.24**	**74.89**	**16.96**
	0.895	24.08	74.86	16.13
	0.902	24.28	74.56	16.33
[b]Average	**0.898**	**24.55**	**74.67**	**16.45**

[a]The device architecture is ITO/PEDOT:PSS/active layer/PNDIT-F3N/Ag; D=4.23 mg/mL in chloroform; the resulting solutions were spin-casted at 2500 rpm for 30 s onto the PEDOT:PSS layer; CS_2 SVA 3min. [b] The average values are obtained from 15 devices.

Table S18. Detailed photovoltaic parameters of the PM6:CH-4Cl based devices by optimal conditions under the illumination of AM 1.5 G, 100 mW cm^{-2}.[a]

Active layer	V_{OC} (V)	J_{SC} (mA cm^{-2})	FF (%)	PCE (%)

	0.903	25.04	76.54	17.32
	0.899	25.33	75.25	17.13
	0.900	25.40	76.31	17.44
	0.899	25.45	76.82	17.58
	0.898	25.36	76.45	17.42
	0.898	25.20	76.65	17.33
	0.900	25.53	75.18	17.28
D18:CH-4Cl	0.898	25.45	75.24	17.20
	0.899	25.24	76.12	17.27
	0.898	**25.59**	**76.83**	**17.65**
	0.897	25.19	76.38	17.26
	0.904	24.94	76.45	17.23
	0.901	25.29	76.15	17.35
	0.900	25.18	76.90	17.43
	0.899	25.19	76.76	17.38
[b]**Average**	**0.900**	**25.29**	**76.27**	**17.35**

[a]The device architecture is ITO/PEDOT:PSS/active layer/PNDIT-F3N/Ag; D=4.23 mg/mL in chloroform; the resulting solutions were spin-casted at 2500 rpm for 30 s onto the PEDOT:PSS layer; CS_2 SVA 3min. [b] The average values are obtained from 15 devices.

Table S19. Detailed photovoltaic parameters of the D18:CH-6Cl based devices by optimal conditions under the illumination of AM 1.5 G, 100 mW cm^{-2}.[a]

Active layer	V_{OC} (V)	J_{SC} (mA cm^{-2})	FF (%)	PCE (%)
	0.903	25.21	74.93	17.06
	0.900	25.02	74.79	16.85
	0.899	25.08	75.43	17.00
	0.898	25.63	74.74	17.20
	0.896	25.68	74.26	17.09
	0.901	25.64	74.00	17.10
	0.899	25.58	74.39	17.11
D18:CH-6Cl	**0.901**	**25.42**	**75.10**	**17.21**
	0.901	25.66	73.81	17.06
	0.901	25.31	74.83	17.06
	0.901	25.04	75.35	17.01
	0.894	25.71	74.00	17.01
	0.895	25.52	75.06	17.14
	0.895	25.19	75.72	17.06
	0.893	25.63	75.15	17.19
[b]**Average**	**0.898**	**25.42**	**74.77**	**17.08**

[a]The device architecture is ITO/PEDOT:PSS/active layer/PNDIT-F3N/Ag; D=4.23 mg/mL in chloroform; the resulting solutions were spin-casted at 2500 rpm for 30 s onto the PEDOT:PSS layer; CS_2 SVA 3min. [b] The average values are obtained from 15 devices.

4. Supporting Notes

Note S1. The reaction mechanism in this work.

In order to explain the reaction mechanism of the crucial conversion from compound **1** to compound **2** in **Fig. 1b**, we have presented the detailed reaction process including two theoretically derived intermediates in **Scheme S5** below.

Firstly, intermediate **1-1** can be afforded through a reduction of compound **1** by using $LiAlH_4$, which has been widely reported.[9, 10]. Secondly, given that compound **1-1** is a very electron-rich system, the diamine on compound **1-1** is extremely easy to be oxidized. Therefore, we selected a high-efficiency dehydrogenation reagent DDQ (2,3-Dichloro-5,6-dicyano-1,4-benzoquinone) to oxidize compound **1-1** into a good electrophile diimine intermediate **1a** (Similar reaction mechanism could be found in literature[11]). Finally, compound **2** can be obtained through a condensation reaction between electrophilic diimine intermediate **1a** and commercial nucleophilic 4,5-dichlorobenzene-1,2-diamine.

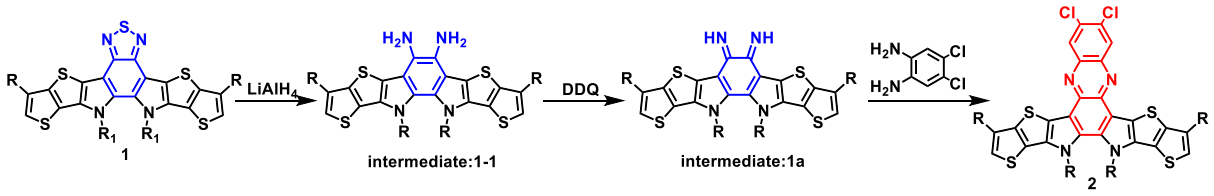

Scheme S5. Explored synthesis routes of the central unit of **CH-6Cl**.

Note S2. Computational methods in this work.

The starting single molecules were taken from their respective single crystals and all the alkyl chains were replaced with methyl groups (-CH_3) to reduce the computational requirements.

The structures were subsequently optimized with Density Functional Theory (DFT) in a vacuum within the Gaussian 16 software.[12] The structure optimization, frequency analysis, energy level of frontier molecular orbital, and the reorganization energy were obtained at the Becke three-parameter Lee-Yang-Parr (B3LYP)[13] hybrid functional with the 6-31G(d)[14] basis set. The electronic coupling between dimers can be obtained by using Prof. Shuai's code based on the equation:[15]

$$\varsigma=\frac{H_{12}-\frac{1}{2}(H_{11}+H_{22})\Sigma_{12}}{1-\Sigma_{12}{}^{2}}$$

Here, $H_{12}=\langle\psi_1|H|\psi_2\rangle$, $S_{12}=\langle\psi_1|\psi_2\rangle$, $H_{11}=\langle\psi_1|H|\psi_1\rangle$, $H_{12}=\langle\psi_2|H|\psi_2\rangle$. H is the Kohn-Sham Hamiltonian of the dimer, $\psi_{1/2}$ means the LUMO of the monomer in the dimer for electron transport, $S_{12}$is the overlap integral. We obtained the transfer integrals at DFT/PW91PW91/6-31G(d) level. Besides, the Mercury software was employed to obtain the total packing energy and the π-π stacking interaction energy were calculated in details.[16, 17]

Note S3. The calculation of miscibility parameters for blend films.

The difference in surface energy (γ) of **PM6**, **CH-6F**, **CH-4Cl**, **CH-6Cl** and **Y6** pure films were applied to obtain the Flory-Huggins interaction parameter χ to explain the degree of molecular miscibility between **CH**-series NFAs and the polymer donor (**PM6**). The surface tension value ($\gamma_{SV}=\gamma_S^d+\gamma_S^P$) can be estimated from the contact angle (θ) according to the Owens-Wendt-Kaelble's model[18]:

$$\gamma_{LV}(1+\cos\theta)=2\left(\sqrt{\gamma_S^P\gamma_L^P}+\sqrt{\gamma_S^d\gamma_L^d}\right)$$

Here, $\gamma_{LV}$is the surface tension of the liquid in equilibrium with its vapor and γ_{SV} is that of the solid. The measured contact angle data were listed in **Figure S29**. The degree of molecular miscibility can be evaluated by Flory-Huggins interaction parameter χ, calculated by formula[19]:

$$\chi_{A:B} = K(\sqrt{\gamma_A} - \sqrt{\gamma_B})^2$$

Note S4. The fitting and calculation details for the E_{CT}

To avoid an arbitrary fitting, two boundary conditions are imposed. Firstly, we have calculated the lower limit for the radiative recombination voltage loss ($V_{r,sq}$) for a solar cell as a function of E_{CT} using the Shockley-Queisser theory, assuming that E_{CT} is the effective energy of the bandgap of an organic solar cell. Then, the Gaussian region in the lower energy part of the EQE spectrum of the solar cell based on **PM6**:**CH**-series is selected and fitted. During the fitting process, a set of *f* values typically in the range between 0.0001 to 0.1 have been used as constant input values, while E_{CT} and λ are left as fit parameters. As a result, we could obtain a range of values for E_{CT}, which are used to calculate ΔV_r, using the simple equation:

$$\Delta V_r = E_{CT}/q - \Delta V_{OC} - \Delta V_{nr}$$

The calculated ΔV_r values are compared to $\Delta V_{r,sq}$ from the Shockley-Queisser theory, and the E_{CT} values leading to ΔV_r smaller than $\Delta V_{r,sq}$ are ruled out. According to that, for example, we could determine the minimal value for E_{CT}, which is 1.370 eV for the solar cell based on **PM6**:**CH-4Cl**:**F-2F**. Then, we have determined the EQE spectrum solely due to CT absorption, using the Marcus equation and the fit results. A loose upper boundary for E_{CT} is that the EQE of CT state absorption should always be lower than the that of the absorption of the singlet states in the solar cell. Therefore, the E_{CT} values giving rise to CT state EQE higher than the EQE of the singlet states are also ruled out. In fact, the CT state EQE should be much smaller than the singlet state EQE, due to the considerably weaker CT state absorption strength. To our knowledge, the highest CT state absorption coefficient in an organic BHJ active layer is found for the intercalated blend system of **PBTTT**:**PCBM**,[20] which is only less than 5% of the singlet absorption coefficient of **PBTTT**. Therefore, for deriving the maximum value of E_{CT} of the

solar cells studied in this work, we could assume that the CT state EQE should contribute less than 10% of the single state EQE. This leads to a maximum value of E_{CT} of 1.372 eV for the solar cell based on **PM6**:**CH-4Cl**:**F-2F**. Therefore, the range of the values for E_{CT} of the solar cell is restricted to 1.371±0.01 eV.

5. ^{1}H and ^{13}C NMR Spectra of the Key Intermediates and Final Products

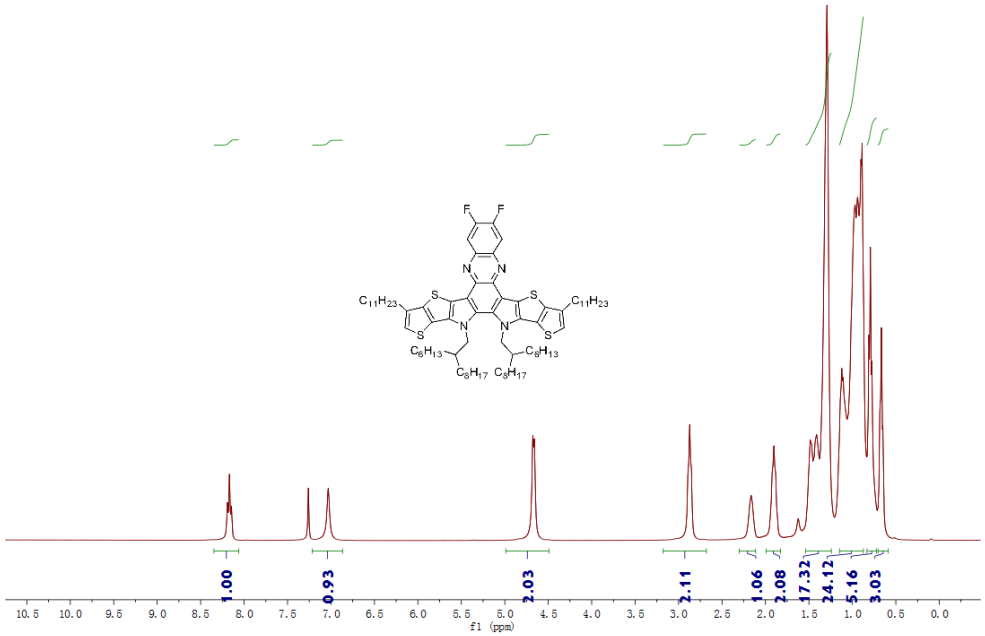

Figure S38. ^{1}H NMR spectrum of compound 2-2F at 300K in $CDCl_3$.

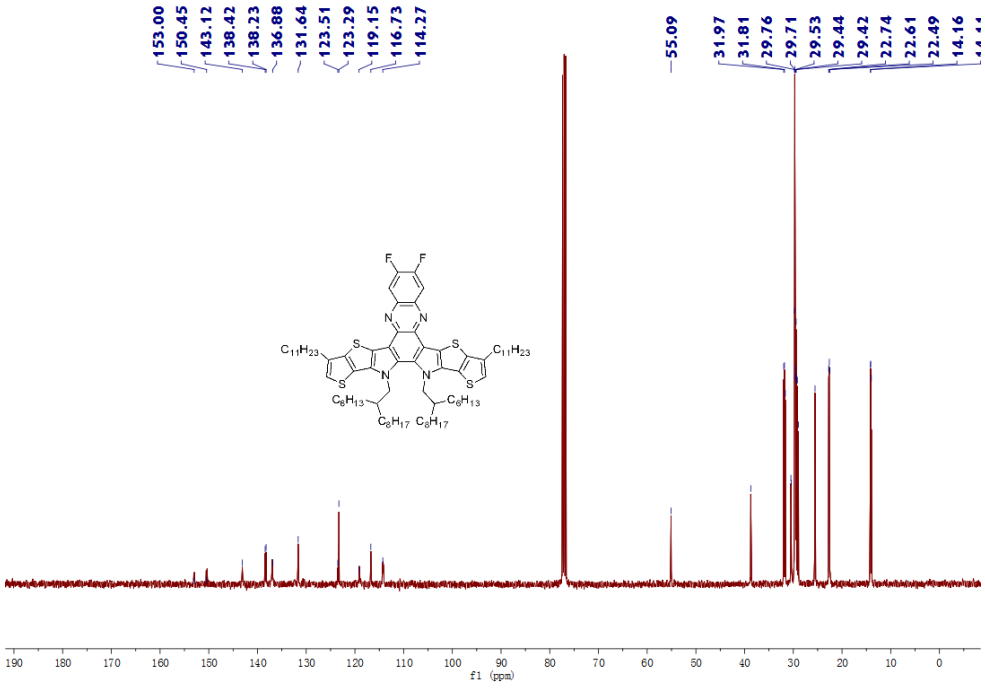

Figure S39. ^{13}C NMR spectrum of compound 2-2F at 300K in $CDCl_3$.

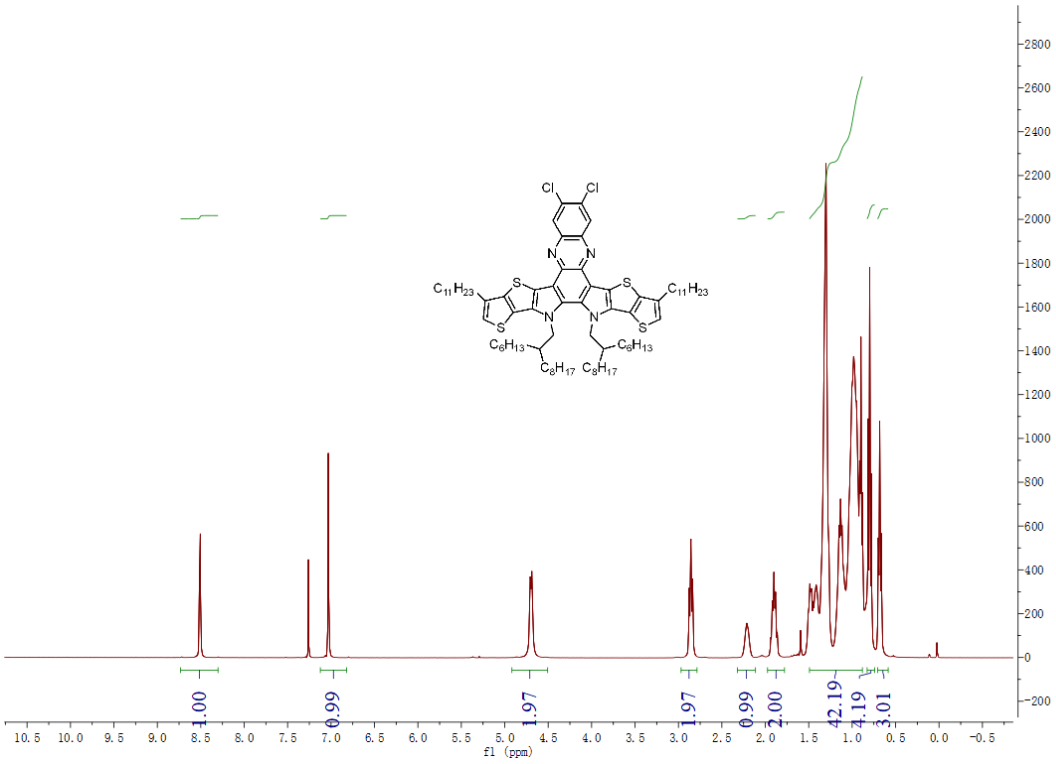

Figure S40. ^{1}H NMR spectrum of compound 2-2Cl at 300K in $CDCl_3$.

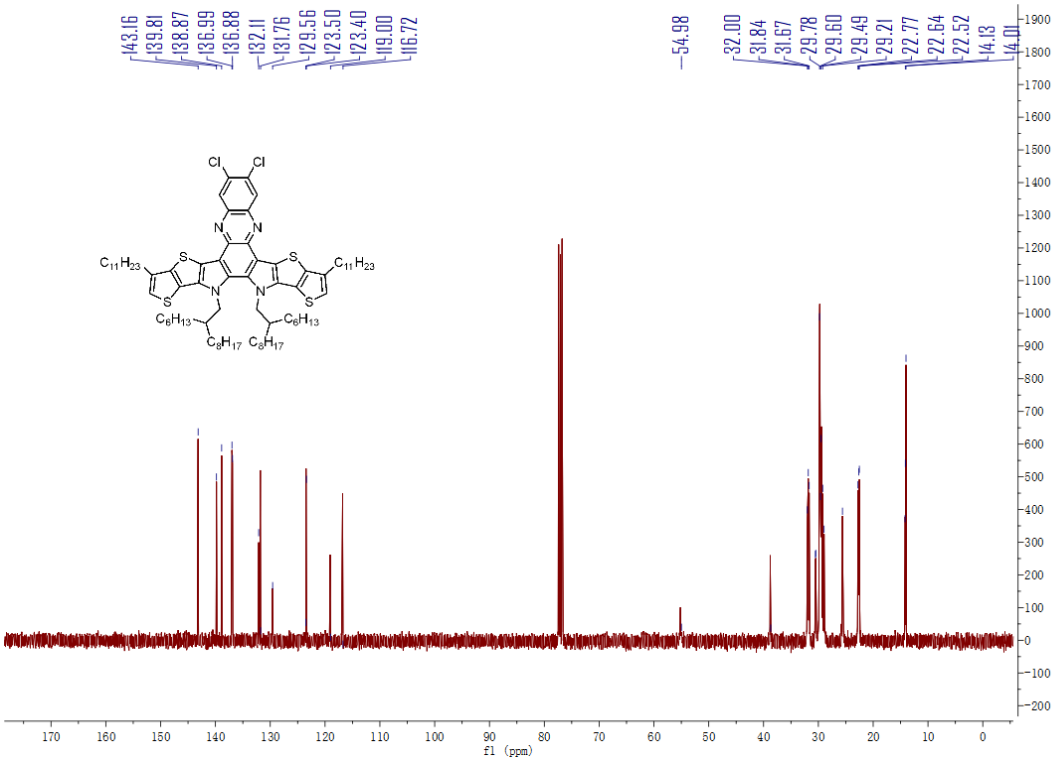

Figure S41. ^{13}C NMR spectrum of compound 2-2Cl at 300K in $CDCl_3$.

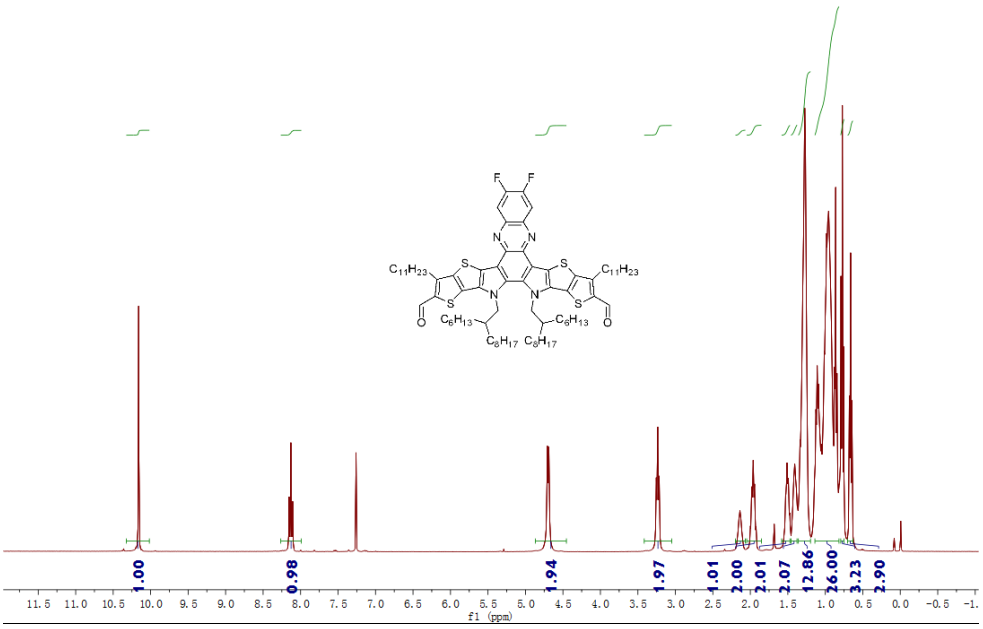

Figure 42. ^{1}H NMR spectrum of compound 3-2F at 300K in $CDCl_3$.

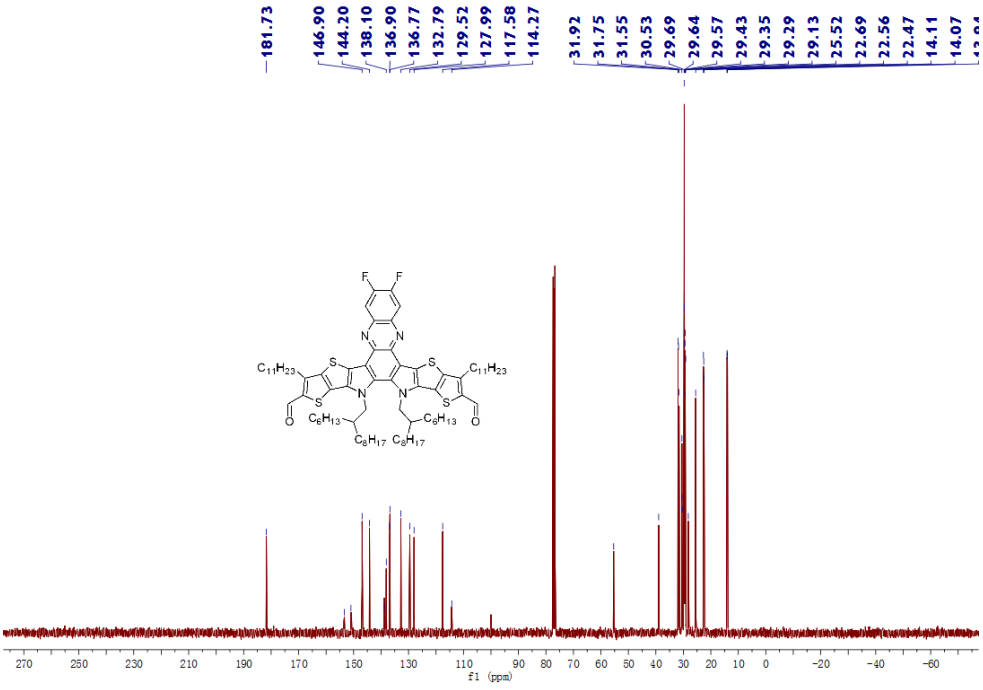

Figure 43. ^{13}C NMR spectrum of compound 3-2F at 300K in $CDCl_3$.

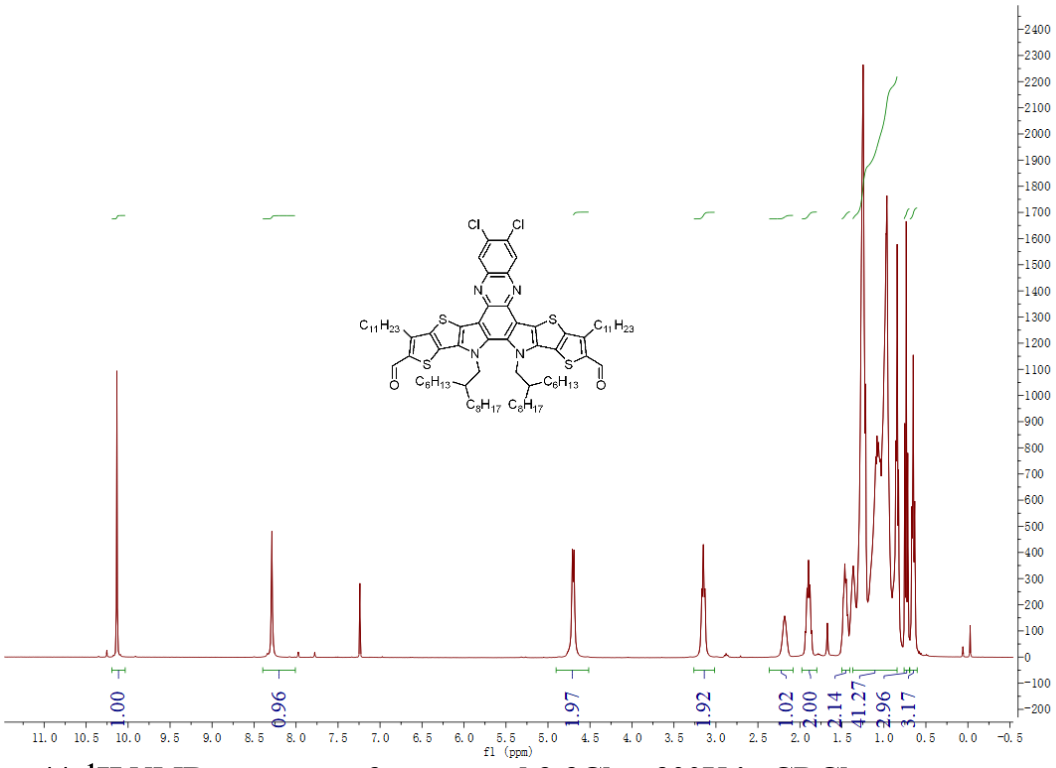

Figure 44. ^{1}H NMR spectrum of compound 3-3Cl at 300K in $CDCl_3$.

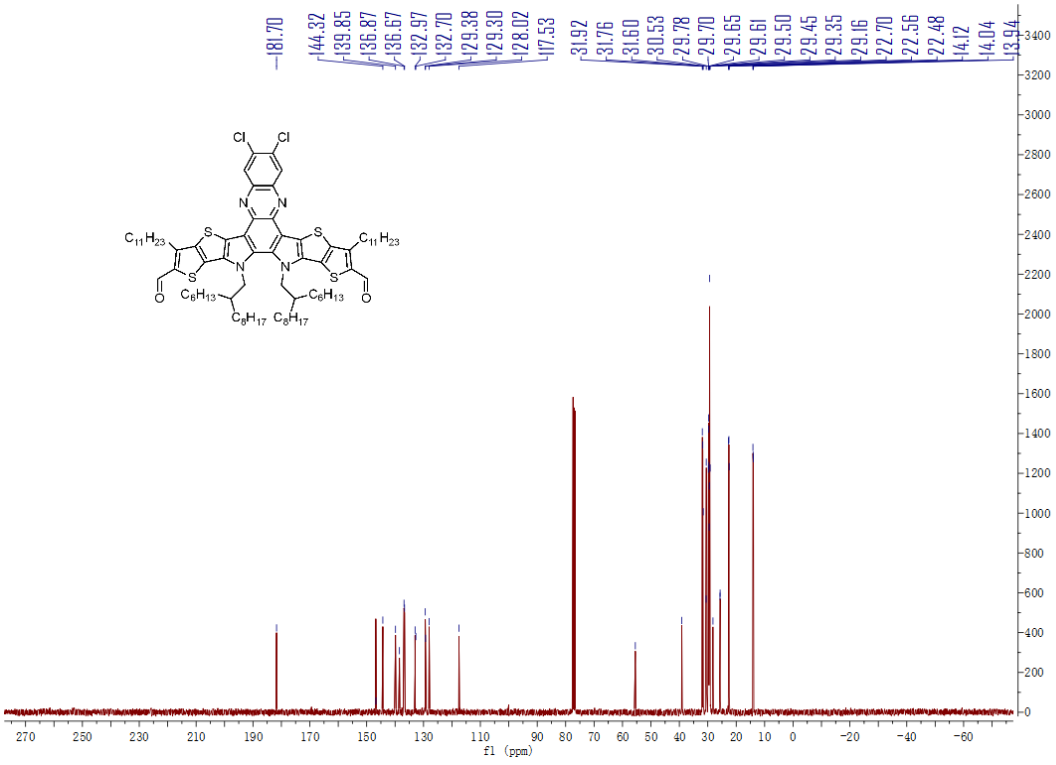

Figure 45. ^{13}C NMR spectrum of compound 3-2Cl at 300K in $CDCl_3$.

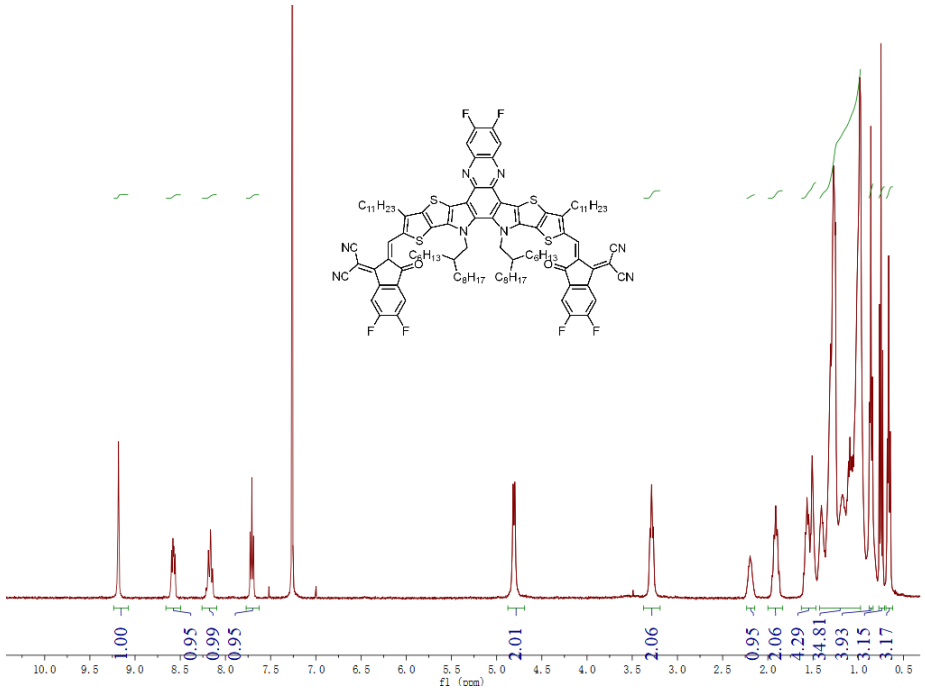

Figure 46. ^{1}H NMR spectrum of CH-6F at 300K in $CDCl_3$.

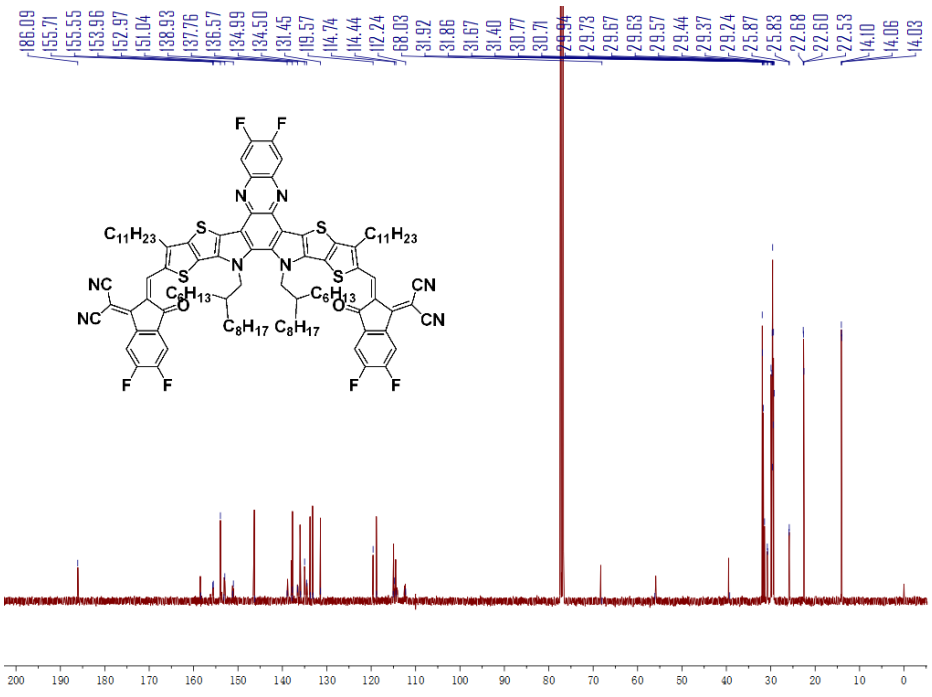

Figure 47. ^{13}C NMR spectrum of CH-6F at 300K in $CDCl_3$.

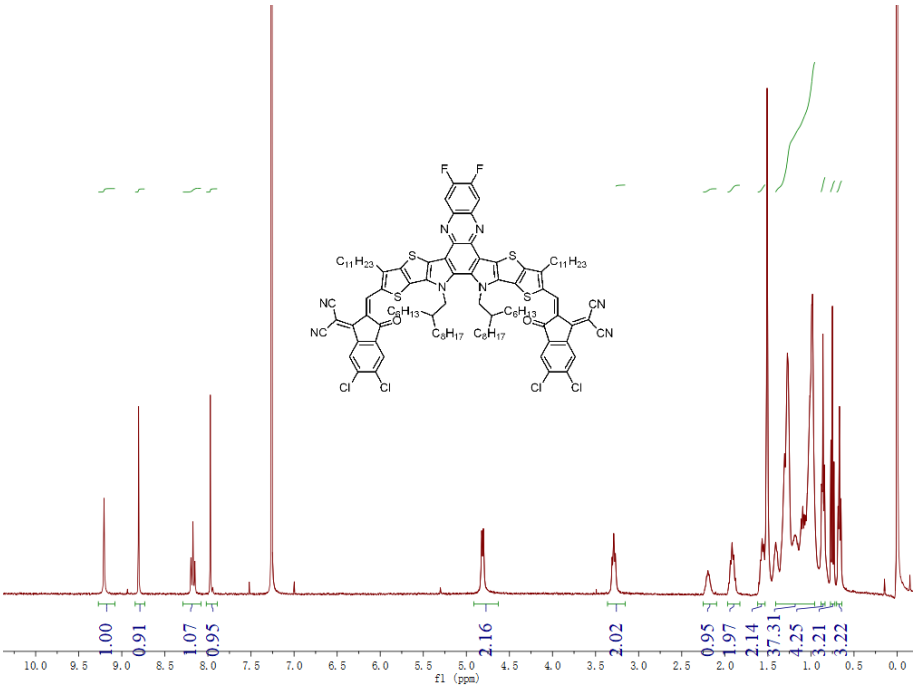

Figure 48. ^{1}H NMR spectrum of CH-4Cl at 300K in $CDCl_3$.

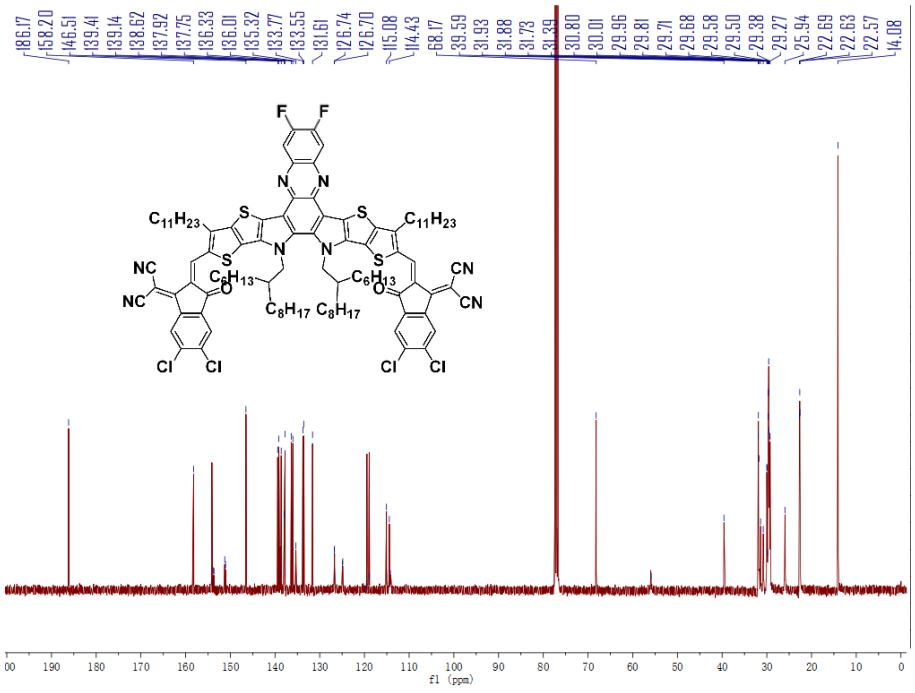

Figure 49. ^{13}C NMR NMR spectrum of CH-4Cl at 300K in $CDCl_3$.

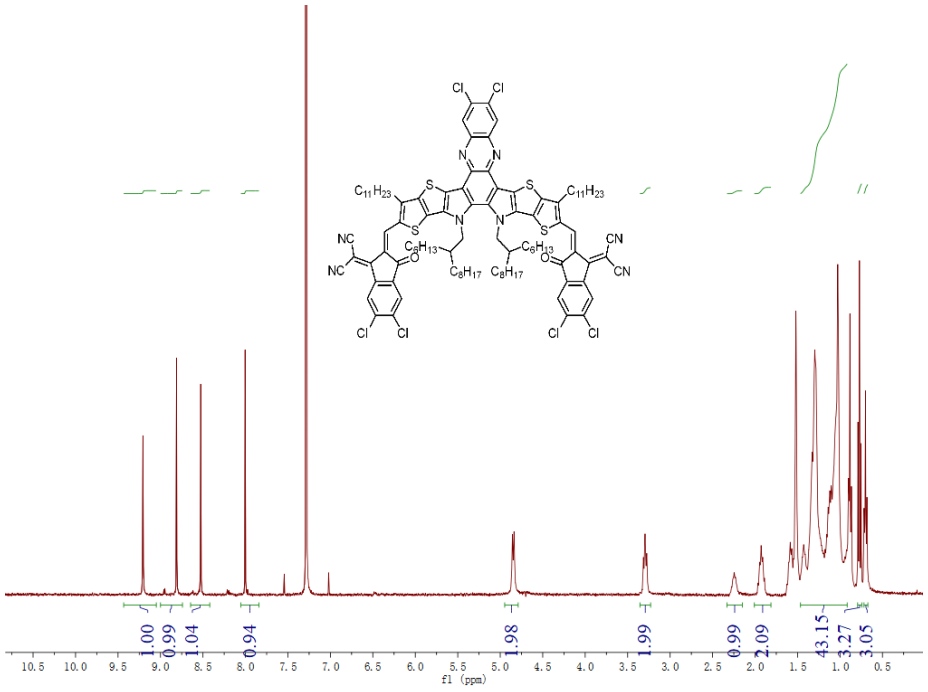

Figure S50. ^{1}H NMR spectrum of CH-6Cl at 300K in $CDCl_3$.

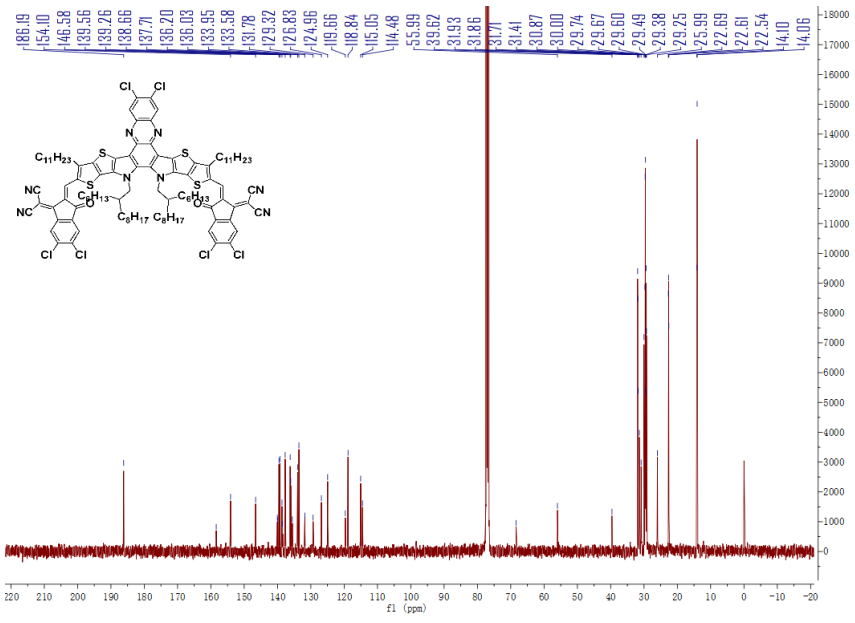

Figure S51. ^{13}C NMR spectrum of CH-6Cl at 300K in $CDCl_3$.

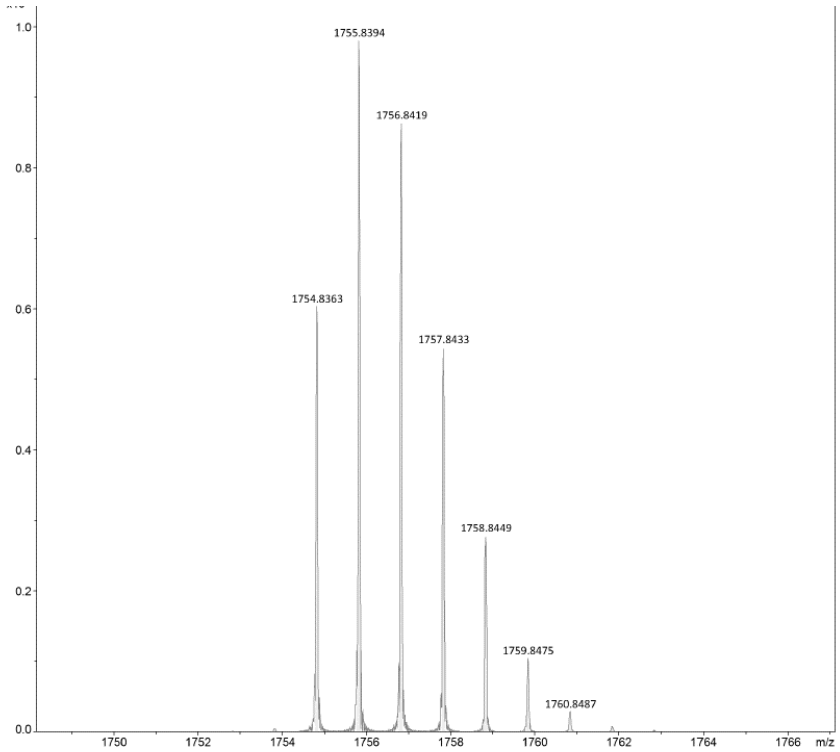

Figure S52. HRMS of CH-6F.

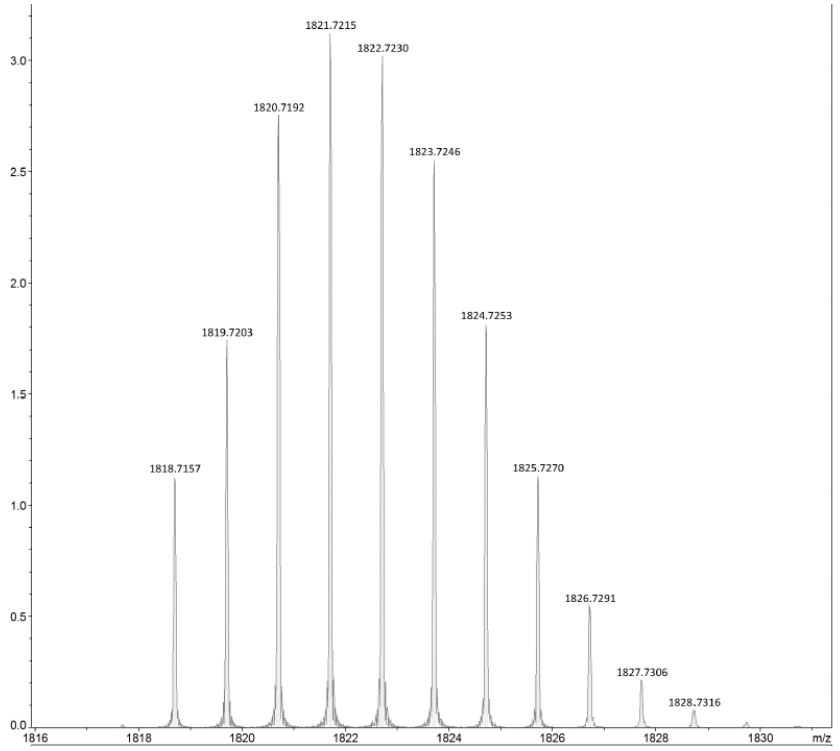

Figure S53. HRMS of CH-4Cl.

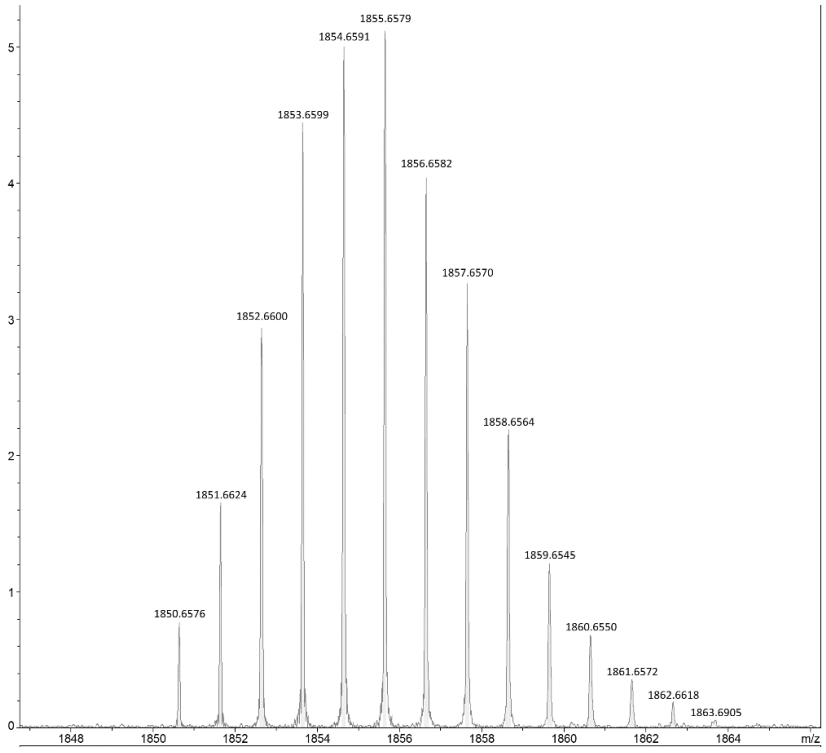

Figure S54. HRMS of CH-6Cl.

References

1. J. Yuan, Y. Zhang, L. Zhou, G. Zhang, H.-L. Yip, T.-K. Lau, X. Lu, C. Zhu, H. Peng, P. A. Johnson, M. Leclerc, Y. Cao, J. Ulanski, Y. Li and Y. Zou, *Joule*, 2019, **3**, 1140-1151.
2. Q. Liu, Y. Jiang, K. Jin, J. Qin, J. Xu, W. Li, J. Xiong, J. Liu, Z. Xiao, K. Sun, K. Sun, S. Yang, X. Zhang and L. Ding, *Science Bulletin*, 2020, **65**, 272-275.
3. X. Ke, L. Meng, X. Wan, M. Li, Y. Sun, Z. Guo, S. Wu, H. Zhang, C. Li and Y. Chen, *J. Mater. Chem. A*, 2020, **8**, 9726-9732.
4. H. Liu, M. Li, H. Wu, J. Wang, Z. Ma and Z. Tang, *J. Mater. Chem. A*, 2021, **9**, 19770-19777.
5. X. Wan, C. Li, M. Zhang and Y. Chen, *Chem. Soc. Rev.*, 2020, **49**, 2828-2842.
6. L. J. A. Koster, M. Kemerink, M. M. Wienk, K. Maturová and R. A. Janssen, *Adv. Mater.*, 2011, **23**, 1670-1674.

7. A. K. K. Kyaw, D. H. Wang, V. Gupta, W. L. Leong, L. Ke, G. C. Bazan and A. J. Heeger, *ACS nano*, 2013, **7**, 4569-4577.

8. Y. Wang, D. Qian, Y. Cui, H. Zhang, J. Hou, K. Vandewal, T. Kirchartz and F. Gao, *Adv. Energy Mater.*, 2018, **8**, 1801352.

9. Z. Zhou, W. Liu, G. Zhou, M. Zhang, D. Qian, J. Zhang, S. Chen, S. Xu, C. Yang, F. Gao, H. Zhu, F. Liu and X. Zhu, *Adv. Mater.*, 2020, **32**, 1906324.

10. C. Zhu, K. An, W. Zhong, Z. Li, Y. Qian, X. Su and L. Ying, *Chem. Commun.*, 2020, **56**, 4700-4703.

11. S. Pascal, L. Lavaud, C. Azarias, A. Varlot, G. Canard, M. Giorgi, D. Jacquemin and O. Siri, *J. Org. Chem.* , 2019, **84**, 1387-1397.

12. M. Frisch, G. Trucks, H. Schlegel, G. Scuseria, M. Robb, J. Cheeseman, G. Scalmani, V. Barone, G. Petersson and H. Nakatsuji, *Inc., Wallingford CT*, 2016, **2016**.

13. A. Becke, *Chem. Phys.*, 1993, **98**, 5648.

14. P. Hariharan and J. A. Pople, *Mol. Phys.*, 1974, **27**, 209-214.

15. L. Wang, G. Nan, X. Yang, Q. Peng, Q. Li and Z. Shuai, *Chem. Soc. Rev.*, 2010, **39**, 423-434.

16. A. Gavezzotti, *Acc. Chem. Res.*, 1994, **27**, 309-314.

17. A. Gavezzotti and G. Filippini, *J. Phys. Chem.*, 1994, **98**, 4831-4837.

18. S. Nilsson, A. Bernasik, A. Budkowski and E. Moons, *Macromolecules*, 2007, **40**, 8291-8301.

19. S. Honda, H. Ohkita, H. Benten and S. Ito, *Adv. Energy Mater.*, 2011, **1**, 588-598.

20. Z. Tang, Z. Ma, A. Sánchez-Díaz, S. Ullbrich, Y. Liu, B. Siegmund, A. Mischok, K. Leo, M. Campoy-Quiles, W. Li and K. Vandewal, *Adv. Mater.*, 2017, **29**, 1702184.